Enhanced and selective translation expands the lysosome size and promotes antigen presentation during phagocyte activation

Victoria E. B. Hipolito[1,2], Jacqueline A. Diaz[2], Kristofferson V. Tandoc[3,4], Neha Chauhan[2,7], Amra Saric[1,8], Ivan Topisirovic[3,4,5,6], and Roberto J. Botelho[1,2*]

[1]Graduate Program in Molecular Science and [2]Department of Chemistry and Biology, Ryerson University, Toronto, Ontario, M5B2K3, Canada

[3]Department of Experimental Medicine, McGill University, [4]The Lady Davis Institute, Jewish General Hospital, [5]Gerald Bronfman Department of Oncology and [6]Department of Biochemistry, Montréal, Quebec H3T 1E2, Canada

[7]Currently in the Graduate Program in Department of Laboratory Medicine and Pathobiology, University of Toronto, Toronto, Ontario, M5S 3H7, Canada

[8]Currently in Cell Biology and Neurobiology Branch, Eunice Kennedy Shriver National Institute of Child Health and Human Development, National Institutes of Health, Bethesda, MD 20892

Running title: Lysosome expansion and translation

*Corresponding author: rbotelho@ryerson.ca

Keywords

Organelles, lysosomes, biogenesis, phagocytes, innate immunity, antigen, membranes, mTOR, translation

Abbreviations

BMDM: Bone marrow-derived macrophages, BMDC: bone marrow-derived dendritic cells; LPS: lipopolysaccharides; LY: Lucifer yellow; PFA: paraformaldehyde; SIM: structured illumination microscopy; 5' TOP: 5' terminal oligopyrimidine; V-ATPase: vacuolar H^+ ATPase pump

Summary

The mechanisms that govern organelle remodeling remain poorly defined. Lysosomes degrade cargo from various routes including endocytosis, phagocytosis and autophagy. For phagocytes, lysosomes are a kingpin organelle since they are essential to kill pathogens and process and present antigens. During phagocyte activation, lysosomes undergo a striking reorganization, changing from dozens of globular structures to a tubular network, in a process that requires the phosphatidylinositol-3-kinase-AKT-mTOR signalling pathway. Here, we show that lysosomes undergo a remarkably rapid expansion in volume and holding capacity during phagocyte activation. Lysosome expansion was paralleled by an increase in lysosomal protein levels, but this was unexpectedly independent of TFEB and TFE3 transcription factors, known to scale up lysosome biogenesis. Instead, we demonstrate a hitherto unappreciated mechanism of acute organelle expansion via mTORC1-dependent increase in translation of mRNAs encoding key lysosomal proteins including LAMP1 and V-ATPase subunits, which is necessary for efficient and rapid antigen presentation by dendritic cells. Collectively, we demonstrate a previously unknown and functionally relevant mechanism of rapid lysosome expansion, whereby mTORC1 senses stimuli to remodel lysosomes via modulating translation of mRNAs encoding key lysosomal proteins.

Introduction

Eukaryotic cells compartmentalize a wide-range of biochemical functions within membrane-bound organelles such as the endoplasmic reticulum, peroxisomes and lysosomes. These organelles can exist in disparate morphologies ranging from individual vesicular organelles, stacks of flattened membrane sacs, to a continuous membrane reticulum. Despite this complexity, cells must control organelle number, size, shape and activity to meet the needs of their differentiation state. In addition, cells must adapt these organellar properties in response to intrinsic and extrinsic stimuli that alter the metabolic and functional needs of cells[1–5]. Yet, how cells determine organellar properties in response to differentiation state and/or changes in their environment remains one of the most outstanding questions in cell biology.

Immune cells like macrophages and dendritic cells are highly plastic inasmuch as they can adopt "resting", highly inflammatory, and anti-inflammatory states that differ in their gene expression profile, metabolic programming, secretory pathway activity and endolysosomal membrane system[6–10]. With respect to the endolysosomal system, mature dendritic cells abate the degradative capacity of their lysosomal system, which is commonly referred to as the MHC-II compartment, to help preserve antigenic peptides for presentation to adaptive immune cells[11]. On the other hand, macrophages enhance their lysosomal degradative power after phagocytosis to enhance bacterial killing[12]. Perhaps, one of the most striking examples of endolysosomal remodelling occurs during lipopolysaccharide (LPS)-activation of macrophages and dendritic cells, which transform lysosomes from a collection of dozens of individual globular organelles into a striking tubular network[10,13,14]. This reorganization requires downstream TLR4 signals including the phosphatidylinositol 3-kinase-AKT-mTOR axis, which may interface with the lysosomal Rab7 and Arl8b GTPases to control lysosome association with microtubule-motor proteins[14,15]. These motors then help distort and tubulate lysosomes on microtubule tracks[13,16,17]. While lysosome tubulation is associated with retention of pinocytic cargo, exchange of phagosomal cargo, and possibly antigen presentation[18–22], it is not presently known how lysosome tubulation helps phagocytes perform their function in response to LPS and other stimulants.

Lysosomes themselves serve as signaling platforms to sense the metabolic and nutrient state of the cell[23–25]. For instance, a protein network involving the V-ATPase, Ragulator and Rag GTPases sense high levels of amino acids within lysosomes to activate mTORC1 on the lysosome surface[26–31]. Active mTORC1 then phosphorylates various downstream targets to stimulate

anabolic pathways, including mRNA translation[32–34]. In part, mTORC1 promotes translation by phosphorylating and activating the S6 kinases (S6Ks), which then act on multiple targets to modulate translation initiation, elongation and ribosome biogenesis[35–38]. This is coordinated by mTORC1-dependent phosphorylation of 4E-BPs which leads to their dissociation from eIF4E, thus allowing the eIF4F complex assembly and the recruitment of the mRNA to the ribosome [36,38,39]. Importantly, mTORC1-driven anabolic pathways are also coordinated with mTORC1-mediated repression of catabolic processes including autophagy. This is in large part achieved by phosphorylating ULK1, an initiator of autophagy, and inhibiting the transcription factor TFEB, which can up-regulate expression of lysosomal genes[40–43]. Inactivation of mTORC1 (e.g. during starvation) initiates autophagy, which is paralleled by a boost in lysosomal gene expression, and lysosomal activity to augment macromolecular turnover and help replenish the nutrients[42,43]. mTORC1 also plays roles that are beyond coordinating anabolism and catabolism in the context of nutrient sensing. In immune cells, these include responding to toll-like receptor ligands like LPS, *Salmonella* invasion, phagocytosis and inflammasome activators[12,15,44,45], though the functional consequences of this phenomenon are not entirely clear.

Herein, we set out to dissect the mechanisms underlying the reorganization of the endolysosomal system in activated immune cells. We discovered that the lysosomal volume and retention capacity is rapidly amplified in LPS-activated phagocytes relative to their resting counterparts. We demonstrated that this expansion depends on augmented *de novo* protein synthesis, but that this is unexpectedly independent of transcriptional mechanisms such as activation of TFEB and TFE3. Instead, LPS-driven lysosomal expansion depends on mTORC1-dependent selective and enhanced translation of lysosomal protein-encoding mRNAs. Moreover, we showed that these effects are mediated via S6Ks and 4E-Bs. Ultimately, we present evidence that mTORC1- and translation-dependent increase in lysosome size and holding capacity is critical for efficient and rapid antigen presentation by dendritic cells.

Results

Activation of macrophage and dendritic cells expands the lysosome volume

Activation of macrophages and dendritic cells elicits a remarkable remodelling of lysosome morphology, converting these organelles from dozens of individual puncta into a tubular network[15,18–20]. Upon careful visual inspection, we speculated that this tubular lysosome network

occupied a larger volume than punctate lysosomes in resting cells (Fig. 1a). To test this, we quantified the total lysosome volume in LPS-activated and resting cells by employing image volumetric analysis [46,47]. We first pre-labelled lysosomes (see materials and methods) with a fluorescent fluid-phase marker and then exposed cells to LPS or vehicle-alone for 2 h to induce lysosome remodelling (Fig. 1a). Pre-labelling cells prior to stimulation ensured that lysosomes are equally loaded with the dye in both resting and activated cells. We then employed live-cell spinning disc confocal microscopy to acquire z-stacks and undertake volumetric analysis. Using this methodology, we observed a significant increase in volume occupied by the fluorescent probe in LPS-stimulated RAW macrophages, bone marrow-derived macrophages (BMDM) and bone marrow-derived dendritic cells (BMDCs) relative to their resting counterparts (Fig. 1b). This suggests that activated phagocytes have an expanded total lysosome volume relative to resting cells.

We previously demonstrated that in RAW macrophages, lysosome tubules were more mobile than punctate lysosomes [13]. Thus, to exclude the possibility that the increase in lysosome volume was due to a trailblazing effect during Z-stack image acquisition, we sought to estimate lysosome volume in fixed cells. However, typical fixation protocols with 4% PFA causes tubular lysosomes to disintegrate (Fig. S1a, b). To circumvent this issue, we developed a fixation procedure that preserves lysosome tubules in macrophages (Fig. S1a, b). Re-applying volumetric analysis to fixed RAW cells, we still observed a significant increase in lysosome volume in activated cells relative to resting phagocytes (Fig. 1c). Finally, to exclude that the increase in lysosome volume is an artifact of the limit of resolution of spinning disc confocal microscopy, we employed structured illumination microscopy (SIM) which enables imaging in super-resolution [48]. Due to limitations of the available SIM system, we sampled three x-y planes centred at the mid-point of cells and quantified the area occupied by the fluid-phase marker (Fig. S1c). This approach also demonstrated a significant increase in label volume in activated RAW, primary macrophages, and BMDCs relative to their resting counterparts (Fig. 1d). These data demonstrate that the lysosome volume expands in response to macrophage and dendritic cell stimulation, concurrent with tubulation.

Phagocyte activation increases lysosomal holding capacity

An expanded lysosome volume may as a corollary lead to a boost in the storage capacity of lysosomes. Hence, we assessed whether activated phagocytes have a higher lysosomal holding capacity relative to resting cells by allowing cells to internalize fluorescent pinocytic tracers to saturation. Indeed, both primary and RAW macrophages pre-activated with LPS exhibited a large increase in fluid-phase accumulation relative to their resting counterparts at each time point examined (Fig. 2a, b; Fig. S2a). We also observed that pre-activated primary macrophages displayed faster rates of pinocytic uptake relative to resting macrophages (Fig. 2c). In fact, the rate of pinocytic uptake was augmented within 15 min of LPS exposure as indicated by macrophages concurrently undergoing pinocytosis and stimulation (Fig. 2c). In comparison, we showed that resting and activated primary macrophages did not differ significantly in the rate of depletion of the pinocytic tracer (Fig. 2d), suggesting that exocytosis rates were similar. RAW macrophages exhibited slightly different dynamics in that the rates of uptake and retention were similar between resting and LPS-stimulated cells (Fig. S2b, S2c). Collectively, these data indicate that activated macrophages have a higher lysosome holding capacity relative to resting macrophages. Lastly, we questioned whether dendritic cells would benefit from an increase in lysosome volume since they are reported to arrest endocytosis after maturation [49,50]. Of note, most reports examine dendritic cell function over 16 h post-stimulation, while recent work shows that mature cells can still endocytose extracellular cargo [51–53]. Importantly, we show here that dendritic cells retained their pinocytic capacity up to 8 h post-activation, which fits the timeline of lysosome reorganization and expansion (Fig. S2d). This suggests that rapidly expanding the lysosome volume may help dendritic cells accumulate more pinocytic content including antigenic material. Overall, our observations are consistent with previous reports suggesting that tubulation in activated macrophages may aid in retaining fluid phase and that mature dendritic cells continue to engulf extracellular material [18,51,52,54].

Activated macrophages express higher levels of lysosomal proteins

Thus far, the data presented here suggest that activated phagocytes rapidly expand their lysosome volume and retention capacity. Though other mechanisms like increased endosomal membrane influx may contribute to this, we postulated that lysosomal biosynthesis may be a significant driver of lysosome expansion during phagocyte activation. To address this hypothesis, we determined the levels of select lysosomal proteins, namely LAMP1, V-ATPase subunits and cathepsin D by

Western blotting in resting and activated primary macrophages. Specifically, we compared resting macrophages to those continuously exposed to LPS for 2 h or 6 h or for 2 h with LPS followed by a 4 h chase with no LPS. In all cases, LPS induced approximately 2-fold induction of LAMP1 and V-ATPase subunits H and D protein as compared to resting macrophages (Fig. 3a, b). In contrast, cathepsin D levels were unchanged (Fig. 3a, b), suggesting that LPS exerts differential effect on lysosomal proteins. The increase in LAMP1, ATP6V1H and ATP6V1D was blunted by the translation elongation inhibitor, cycloheximide, indicating that *de novo* protein synthesis, rather than lower protein turnover, augments the levels of lysosomal proteins in LPS-treated phagocytes (Fig. 3a, b). Importantly, cycloheximide blunted lysosome tubulation and expansion in macrophages in response to LPS (Fig. 3c, d). Overall, our data support a role for *de novo* protein synthesis in remodelling and expanding the lysosome network during phagocyte activation.

Rapid lysosome expansion is not dependent on TFEB and TFE3

Our results suggest that biosynthesis plays a major role in LPS-induced lysosome expansion in macrophages. Activation of TFEB and TFE3 transcription factors drives expression of lysosomal genes thereby stimulating lysosome function under various stresses including starvation, phagocytosis, protein aggregation and macrophage activation [12,42,55–61]. Thus, we next investigated whether the observed rapid lysosome expansion was driven by TFEB- and TFE3-mediated transcriptional upregulation of lysosome genes.

To assess activation of TFEB and TFE3, we quantified nuclear translocation by determining the nucleocytoplasmic ratio of endogenously expressed proteins by immunofluorescence [12,62]. As expected, resting cells exhibited mostly cytoplasmic TFEB and TFE3, whereas inhibition of mTOR for 1 h with torin1 caused both proteins to translocate into the nucleus (Fig. 4a, b). Strikingly, while 2 h incubation with LPS rapidly induced lysosome remodelling and expansion, this did not trigger nuclear translocation of TFEB or TFE3 (Fig. 4a, b). In comparison, a prolonged 6 h incubation with LPS initiated nuclear entry of these proteins, especially for TFE3 that was comparable to mTOR suppression (Fig. 4a, b). These results are consistent with observations by Pastore *et al.,* who also observed delayed nuclear entry of these proteins in response to LPS-induced macrophage activation [59]. Strikingly, mRNA levels of TFEB and TFE3 target genes (i.e. LAMP1, TRPML1 and two V-ATPase subunits) were not increased

even after 6 h of LPS exposure (Fig. 4c), whereas there was massive upregulation of interleukin-6 mRNA (Fig. 4d).

To further exclude the role of TFEB in lysosome expansion during macrophage activation, we measured tubulation and lysosome volume in RAW macrophages deleted for the genes encoding TFEB and/or TFE3 using CRISPR-based technology [59]. Deletion of TFEB and TFE3 did not significantly affect LAMP1 protein levels under resting conditions (Fig. S3a, b) nor fluid-phase marker trafficking, as quantified by Mander's coefficient for dextran-containing LAMP1 signal (Fig. S3c, d). Moreover, both resting wild-type and deletion strains of RAW macrophages accumulated similar levels of the dextran probe after 1 h of uptake and 1 h chase (Fig. S3e). Finally, TFEB and TFE3 status in the cell did not exert major influence on retention of the fluid-phase probe after 2 h of LPS exposure (Fig. S3f). Collectively, these data suggest that TFEB and/or TFE3 have minimal impact on basal lysosome biogenesis, basal pinocytosis and trafficking to lysosomes.

We next examined remodelling of lysosomes by treating wild-type and TFEB and/or TFE3-deleted RAW cells with LPS for up to 2 h. Importantly, all three mutant cell lines exhibited a significant increase in lysosome tubulation after 2 h of LPS treatment relative to resting condition. This increase in lysosome tubulation in cells depleted of TFEB and/or TFE3 was indistinguishable from that observed in control, TFEB and TFE3 proficient cells (Fig. 4e). Moreover, LPS-induced expansion of the total lysosome volume was comparable between control and TFEB and/or TFE3-deleted cells (Fig. 4f). Surprisingly, these results suggest that TFEB and/or TFE3-dependent transcription-based program is not a major driver for the rapid lysosome expansion during acute macrophage activation.

Rapid lysosome expansion depends on AKT and mTOR activity

Given that the levels of lysosomal proteins, but not corresponding mRNAs were induced by LPS treatment, we next studied the role of mRNA translation in lysosome expansion. Activated macrophages exhibit extensive metabolic reorganization, enhanced protein synthesis, selective translation of mRNAs encoding inflammatory proteins, and activation of unfolded protein response[6,8,9,63,64]. Consistently, LPS activates mTORC1 in macrophages, which not only stimulates mRNA translation, but is also necessary for lysosome tubulation[15,33,34]. Thus, we tested whether mTOR activity is necessary for enhanced lysosome volume and holding capacity. Indeed,

both primary and RAW macrophages exhibited increased phosphorylation of mTORC1 substrates S6K and 4E-BP1 after exposure to LPS, which is blunted by torin1, which acts as active-site mTOR inhibitor (Fig. 5a, b). Moreover, consistent with our previous observations [15], lysosome tubulation was suppressed upon inhibition of mTOR or AKT by torin1 and Akti, respectively (Fig. 5c). Importantly, suppression of AKT and mTOR activity abrogated the LPS-induced expansion of the lysosome volume (Fig. 5d). Finally, the increase in the holding capacity for pinocytic fluid enticed by LPS treatment was blunted by torin1 (Fig. 5e). Collectively, these findings demonstrate that mTOR is stimulated by LPS, whereby mTOR activation is required for an increase in lysosome holding capacity, volume expansion and tubulation.

In response to LPS, mTOR selectively increases translation of mRNAs encoding lysosomal proteins

Given that mTOR is hyperactivated in LPS-exposed phagocytes and its activity is necessary for lysosome expansion, we next tested whether LPS stimulates global protein synthesis in primary macrophages by employing the puromycylation assay. LPS enhanced puromycin incorporation as compared to control in a time-dependent manner, which is indicative of elevated protein synthesis (Fig. 6a, b). Torin1 abrogated the LPS-induced increase in puromycylation (Fig. 6a, b). As a positive control, we demonstrated that translation elongation inhibitor cycloheximide abrogated puromycylation (Fig. 6a, b). Altogether, these results demonstrate that LPS bolsters global protein synthesis in primary macrophages.

In addition to regulating global protein synthesis rates, changes in mTOR activity cause selective alterations in translation of specific mRNA subsets [65]. Considering that LPS increased lysosomal protein levels without altering their stability or corresponding mRNA abundance (Fig. 3a and 4c), we next postulated that mTOR stimulates lysosome expansion by inducing translation of mRNAs encoding lysosomal proteins. To test this hypothesis, we employed polysome profiling wherein mRNAs are separated according to the number of bound ribosomes by sedimentation through the 5-50% sucrose gradient[66]. Distribution of mRNAs encoding lysosomal proteins across the gradient was measured by RT-qPCR. Due to technical limitations related to the amount of the material required for polysome profiling studies, these experiments were carried out using RAW macrophages. Relative to the control, LPS treatment shifted the distribution of mRNAs encoding LAMP1, and the V-ATPase subunits H and D towards the heavy polysome fractions, which is

indicative of increased translational efficiency (Fig. 7a-c and Sup. Fig. S5). Importantly, although torin1 exerted minimal effect on the distribution of LAMP1 and V-ATPase subunits H and D mRNAs in control cells (Sup. Fig. S4), it dramatically reduced loading of these transcripts on heavy polysomes in LPS treated cells (Fig. 7a-c, Sup. Fig. S5). These findings indicate that LPS induces translation of mRNAs encoding LAMP1, and V-ATPase subunits H and D via mTOR. Of note, translational regulation of LAMP1 and V-ATPase subunits H and D is further buttressed by the results obtained in primary macrophages wherein LPS treatment induced LAMP1 and V-ATPase subunits protein levels, without affecting their mRNA levels or protein stability (Fig. 3a and 4c). In striking comparison, distribution of mRNAs encoding the two heavy polysomal housekeeping proteins β-actin and PPIA remained unchanged upon addition of LPS and/or torin1 (Fig. 7d, e, and Sup. Fig. S5). β-actin and peptidylpropyl isomerase A (PPIA) are housekeeping proteins which are not affected by LPS exposure [67,68]. Similarly, the light polysomal housekeeping protein β2-microglobulin (B2M), was insensitive to both mTOR and LPS signals (Fig. 7f and l, Sup. Fig. S5). Collectively, these observations show that translation of mRNAs encoding lysosomal proteins is selectively stimulated during macrophage activation by LPS in an mTOR-dependent manner.

4E-BP1 and S6 kinase regulate lysosome expansion in activated phagocytes

mTORC1 enhances mRNA translation through multiple mechanisms[36]. Given that LPS stimulates mTORC1, leading to phosphorylation and activation of S6K and repression of 4E-BPs (Fig. 5), we next tested whether these translation regulatory factors play a direct role in LPS-induced lysosome expansion. To disrupt S6 kinase function in primary macrophages, we used LY258470, a potent pharmacological inhibitor of S6 kinase (Fig. S6A). We showed that LY258470 treatment of primary macrophages abrogated LPS-induced lysosome volume increase (Fig. 8a, c), but not lysosomal tubulation (Fig. 8b), which suggest a previously unrecognized uncoupling lysosome tubulation and expansion. Similarly, inhibition of S6 kinases thwarted the LPS-mediated increase in the levels of LAMP1, ATP6V1H and ATP6V1D (Fig. 8d, e). LY258470 had no effect on lysosomal transcript levels in resting cells or those co-exposed with LPS (Fig. S6b). Together, these data suggest that the mTORC1-S6 kinase axis promotes lysosomal protein expression to rapidly expand the lysosome size during phagocyte activation.

We next investigated the role of 4E-BPs in regulating lysosome expansion following LPS. For this, we generated RAW macrophages that stably expressed 4E-BP1^{4Ala}, a phosphorylation-deficient mutant of 4E-BP1 carrying alanine substitutions at four phosphorylation sites (Thr37, Thr46, Ser65, and Thr70), rendering it inaccessible to mTORC1 regulation[69]. This form of 4E-BP1 constitutively binds to a cap-binding protein eIF4E which prevents the assembly of the eIF4F complex thereby hindering recruitment of the mRNA to the ribosome[69]. First, relative to resting RAW counterparts, we showed that LPS augmented the lysosomal volume and lysosome tubulation in RAW cells expressing an empty pBabe retroviral vector (Fig 9a-c). In sharp contrast, LPS failed to boost the lysosome volume in RAW cells that stably expressed 4E-BP1^{4Ala}, though lysosome tubulation still occurred (Fig. 9a-c). Second, changes in lysosome volume were accompanied by corresponding alterations in lysosomal protein levels. Indeed, LPS exposure increased lysosomal protein levels (LAMP1, ATP6V1H and ATP6V1D) in RAW cells expressing the empty retroviral vector, compared to resting counterparts (Fig 9d, e). In contrast, LPS failed to boost the levels of these proteins in RAW cells stably expressing 4E-BP1^{4Ala} (Fig. 9d, e). Collectively, these data reveal that the effects of mTORC1 on lysosome remodeling are mediated via orchestrated activity of S6Ks and 4E-BPs.

Antigen presentation is promoted by LPS through mTOR and S6K activity

Our results thus far suggest that LPS induces a rapid lysosomal expansion in primary phagocytes via mTOR-dependent boost in translation of lysosomal transcripts. Next, we sought to investigate the functional implication of LPS-mediated escalation in translation and lysosomal volume. We postulated that LPS-mediated lysosome expansion and increase in holding capacity may enhance antigen presentation by BMDCs. To test this, we used BMDCs from C57Bl/6 and C3H/He mice that respectively carry MHC-II haplotypes I-A^b and I-A^k. I-A^b and I-A^k expressing BMDCs were then respectively fed antigenic peptides, Eα^{52-68} and Hen Egg Lysozyme (HEL), for 4 and 6 hours in the presence or absence of LPS. We used Aw3.18 monoclonal staining of fixed but unpermeabilized BMDCs to detect surface delivery of I-A^k:: HEL$^{48-62}$ complexes[70] – this antibody could not detect MHC-II:peptide complex after permeabilization (not shown). On the other hand, we could detect total I-A^b::Eα^{52-68} [71] (internal and surface level) complex formation by staining fixed and saponin-permeabilized BMDCs with the monoclonal Y-Ae antibody[71]. Importantly, treatment with LPS stimulated formation and/or delivery of the MHC-II::peptide complexes even

at 4 h and more potently at 6 h (Fig. 10a, c and Supp. Fig. 6c). When cells were not given antigens, signal was reduced to background, demonstrating that the fluorescence signal was dependent on MHC-II::antigen complex formation (Fig. 10c, Sup. Fig. S6c). We then inquired if antigen presentation was dependent on mTOR and S6K activities by co-treating cells with torin1 and LY258470, respectively. Remarkably, these inhibitors reduced antigen presentation of both $E\alpha^{52-68}$ and HEL^{48-62} in unstimulated and LPS-treated cells (Fig. 10b, d and Fig. S6c). These data indicate that enhanced translation controlled by the mTORC1-S6K axis is necessary for efficient antigen presentation by BMDCs. Collectively with all the other observations, we propose that this is in part due to rapid lysosomal expansion and remodelling.

Discussion

Macrophages and dendritic cells are highly plastic inasmuch as they can dramatically alter their metabolic and gene expression profiles to adopt a range of alternative states, which exert both inflammatory or anti-inflammatory functions. Significant attention has been given to how macrophages and dendritic cells alter their metabolism and expression of cytokines, chemokines and other microbicidal agents[6–9]. Remodelling the expression level of these factors occurs both at the transcription and translation level[63,72–74]. However, remarkably less is understood regarding the mechanisms that underpin changes to the endomembrane system during activation of macrophages and dendritic cells. Most notably, changes to the endomembrane system include reduced degradative capacity of endolysosomes to help conserve antigens in dendritic cells, and a dramatic morphological reorganization of the endolysosome system in both cell types, shifting from a large collection of vesicular organelles into a highly tubular network of lysosomes[11,19,20]. Tubular lysosomes are associated with increased pinocytic retention, exchange of phagosomal content within the endolysosomal system, and delivery of MHC-II-peptide for presentation, though how this occurs remains unknown[15,18,19,22,75]. Herein, we show that activated phagocytes also rapidly expand the lysosome volume and holding capacity. We provide evidence that this expansion relies on enhanced and selective translation of lysosome encoding transcripts via the mTORC1-S6K-4E-BP axes. In turn, this seems to enhance antigen retention, leading to efficient antigen presentation.

Re-organization and function of the lysosome system in activated phagocytes

Here, we disclose that activated macrophages and dendritic cells remodel their lysosome system into an expanded tubular network with augmented holding capacity. This conclusion is supported by several observations. First, imaging volumetric analysis revealed that dyes preloaded into lysosomes occupy a greater volume post-LPS activation using both live- and fixed-cell imaging, as well as super-resolution microscopy. Second, there was an increase in the expression level of several lysosomal proteins that was blunted by cycloheximide treatment or when translation was abated. Third, activated macrophages could hold a larger amount of fluid-phase relative to resting counterparts. Thus, overall, activated phagocytes not only undertake morphological reorganization of lysosomes but also expand this organelle. The increase in lysosome volume and holding capacity is consistent with work by Swanson *et al.* done in the 1980s showing that phorbol ester-activated macrophages retain fluid-phase more effectively than resting macrophages [18,54].

Functionally, an expanded lysosome volume may help phagocytes engulf more material and/or process extracellular particulates and soluble cargo more efficiently. This expansion of the endolysosome system should benefit both macrophages and dendritic cells upon activation. While mature dendritic cells are reported to have reduced endocytosis[49,50], we show here that dendritic cells exhibit extensive pinocytosis for at least 8 h post-activation, providing an avenue to internalize and accumulate antigenic material. This is also consistent with recent reports revealing that dendritic cells are still able to internalize significant amounts of extracellular content[51,52]. Consistent with this concept, we showed here that LPS stimulation of BMDCs significantly increased presentation of two distinct antigenic peptides as early as 4-6 h of antigen uptake. Importantly, antigen presentation was highly dependent on mTOR and S6K activities, suggesting that up-regulated translation coupled to lysosome expansion helps drive antigen presentation efficiency. Of course, additional mechanisms may also assist antigen presentation in BMDCs including LPS-mediated alteration of lysosome luminal properties like pH and exocytosis of lysosome tubules, which also depends on mTOR[15,19,20]. The extent of individual contributions made by lysosome tubulation, expansion, secretion and luminal remodeling to antigen presentation will need to be assessed in future studies.

Mechanistic insight into lysosome volume expansion

Phagocyte activation leads to a rapid expansion of lysosome volume within two hours of LPS exposure. This expansion is driven by *de novo* protein synthesis as indicated by cycloheximide-

mediated block in lysosome expansion. Unexpectedly, our data also suggest that rapid expansion of lysosome volume and holding capacity in response to LPS stimulation is not dependent on transcription changes to lysosome protein-encoding genes since we did not observe induction of corresponding mRNA levels even after 6 h post-LPS activation. Consistent with this, kinetics of TFEB and TFE3 translocation into the nucleus did not parallel initial lysosome enlargement. Lastly, deletion of these transcription factors did not impair tubulation or rapid lysosome expansion. In contrast to transcriptional programs, we observed that mTOR-dependent translational mechanisms play a key role in LPS-mediated lysosome expansion. First, LPS activates mTORC1, as indicated by increased phosphorylation of S6K and 4E-BP1, and enhanced protein synthesis, whereas its inhibition abrogated lysosome tubulation and expansion. Second, while the translation machinery is governed by a plethora of mechanisms, including mTOR-independent pathways, our data reveal that S6Ks and 4E-BPs play a major role in governing lysosome size in response to stress. Potentially, mTORC1-mediated inhibition of 4E-BPs releases the translation brake imposed on the translation initiation factor eIF4E[36,76]. On the other hand, the role of S6Ks in this process is potentially more complex given its numerous targets that modulate translation, including the ribosomal protein rpS6, the translation initiator factor eIF4B, PDCD4 which governs the function of eIF4A, eEF2K which governs elongation rates and SKAR that may promote mRNA splicing and maturation[36,77,78]. We propose that mTORC1-regulated mRNA translation is a mechanism that broadly serves to rapidly scale the activity and size of other organelles in response to metabolic alterations and stress. Consistent with this idea, inhibition of TSC1/2, an inhibitor of mTORC1, or overexpression of S6Ks increased the size and length of cilia in *Chlamydomonas reinhardtii* and zebrafish[79].

We also observed that the effects of LPS on translation of mRNAs encoding lysosomal proteins are selective, whereby translation of a subset, but not all lysosomal transcripts is upregulated. It is well accepted that in addition to its effects on global protein synthesis, mTOR selectively increases translation of specific mRNA subsets. Of these, the best characterized mRNAs are those carrying a 5' terminal oligopyrimidine tract (5'TOP) which renders transcript translation mTOR-sensitive[80–83]. However, the lysosomal mRNAs encoding LAMP1 and V-ATPase subunits that were probed here do not contain the classical 5'TOP sequences. This is consistent with recent studies suggesting that a significant number of mTOR-sensitive mRNAs lack the 5'-TOP motif[84–86]. We anticipate that transcripts encoding lysosomal proteins may be a

useful functional model to identify novel mRNA sequence or structural motifs that engender mTOR-dependent translation.

Overall, we demonstrate that activated phagocytes dramatically reorganize their lysosomal system by expanding and forming a tubular lysosome network. This amplifies the lysosome holding capacity of phagocytes, augmenting their ability to internalize and retain more extracellular cargo, likely contributing to enhanced antigen presentation. We demonstrate that this process is rapid and occurs via enhanced and selective translation of mRNAs encoding lysosomal proteins, governed by mTOR, S6K and 4E-BPs. Collectively, we propose that mTORC1 and the regulated translation machinery is an important mechanism employed by cells to scale and adapt the size and volume of organelles in response to stress signals.

Material and Methods

Cell lines and primary cells

Murine RAW macrophage cell lines carrying CRISPR-mediated deletion of TFEB, TFE3 or both were a kind donation from Dr. Rosa Puertollano, NIH, and were previously described[59]. These cells and the wild-type RAW264.7 (TIB-71 from ATCC, Manassas, Virginia) were grown in DMEM supplemented with 5% heat-inactivated fetal bovine serum (Wisent, St. Bruno, Canada) at 37°C with 5% CO_2. BMDCs and bone marrow-derived macrophages (BMDMs) were harvested from wild-type 7-9-week-old female C57BL/6J mice or C3H/HeN mice (Charles River Canada, Montreal, QC) as previously described with minor modifications[87,88]. Briefly, bone marrow was isolated from femurs and tibias through perfusion with phosphate-buffered saline (PBS) using a 27G syringe. Red blood cells were lysed using a hypoosmotic treatment. For BMDCs, cells were plated at 2×10^6/well in 4 ml of DMEM supplemented with 10% fetal bovine serum, 55 μM β-mercaptoethanol, 10 ng/ml recombinant mouse granulocyte-macrophage colony-stimulating factor (PeproTech, Rocky Hill, NJ), and penicillin/streptomycin antibiotics (Wisent). Media was changed every 2 days by replacing half of the medium with fresh medium. For BMDMs, cells were plated according to experimental requirements in DMEM supplemented with 10% fetal bovine serum, 20 ng/ml recombinant mouse macrophage colony-stimulating factor (Gibco, Burlington, ON), and penicillin/streptomycin antibiotics. Media was changed every 2 days. Experiments were conducted on days 7–9. All animals were used following institutional ethics requirements.

RAW 4EBP^{4Ala} stable cell line production

We generated RAW cells stably expressing the HA-4E-BP1 (4Ala) phosphorylation mutant or the corresponding empty pBABE vector as previously described[69], with minor modifications. Briefly, pBABE constructs were transiently transfected into the 293Phoenix-AMPHO packaging cell line using Lipofectamine 2000 (ThermoFisher), as per manufacturer's guidelines. Following 48 h, the viral titer was harvested and passed through a 0.45 μm filter. The virus-containing medium was then used to infect RAWs in the presence of 8 μg/mL polybrene (Sigma-Aldrich) for 24 h. Infection was repeated twice more. Twenty-four hours after the final infection, the medium was supplemented with 3 μg/mL puromycin (Sigma-Aldrich) and cells were selected for 1 week then harvested.

Rate, retention and accumulation of pinocytic probes

To measure pinocytosis rate or the accumulation of pinocytic cargo, BMDMs and RAW macrophages were pulsed with 1 mg/mL Lucifer yellow (ThermoFisher Scientific, Burlington, ON) for the indicated time with and without LPS, or after 2 h of LPS pre-stimulation. For pinocytic retention, BMDMs and RAW macrophages were maintained in resting conditions or stimulated with LPS for 2 h, followed by a 30-min pulse with 1 mg/ml Lucifer yellow. Cells were then washed 3x with PBS, and fresh medium was added for the indicated chase periods. In all cases, cells were then washed in PBS, fixed with 4% PFA for 15 minutes and washed in PBS. The amount of Lucifer yellow in RAW macrophages was then quantified using LSRFortessa X-20 cell flow cytometer (BD Biosciences, Mississauga, ON) in 10,000 cells per condition per experiment. Flow cytometry analysis was performed using FCS Express 5 (De Novo Software, Los Angeles, CA). For primary macrophages, Lucifer yellow-labelled cells were visualized using ImageXpress Micro Widefield High Content Screening System (Molecular Devices, Sunnyvale, CA) by where 3x4 quadrants per well were acquired, and the level of probe was analysed using MetaXpress 6 (Molecular Devices). To analyze the pinocytic capacity of BMDCs following activation, cells were pre-stimulated with LPS for the indicated periods, followed by co-incubation with 50 μg/mL of fluorescent dextran in the remaining 30 min of the treatment. Cells were then washed 3x with PBS and fixed with 4% PFA for 15 minutes. Afterwards, dextran fluorescence was imaged by confocal microscopy and quantified with Volocity 6.3.0 image analysis software (PerkinElmer, Bolton, ON) by integrating intensity of dextran.

Lysosome labelling and tubulation

For lysosome labeling, cells were pulsed with 50-100 µg/ml Alexa^{546}-conjugated dextran (ThermoFisher) for 0.5-1 h, followed by 3x wash with PBS and incubated with fresh medium for at least 1 h. To induce lysosome remodeling, BMDMs and BMDCs were exposed to 100 ng/mL LPS from *Salmonella enterica* serotype minnesota Re 595 (Sigma-Aldrich, Oakville, ON), while RAW macrophages were incubated with 500 ng/mL for 2 hours (unless otherwise stated). For pharmacological inhibition, cells were pre-incubated for 15-20 minutes with 100 nM torin1 (Tocris Bioscience, Minneapolis, MN), 10 µM cycloheximide (Bio-Shop), 1 µM LY2584702 (Selleck Chemicals, Houston, TX) or equivalent volume of vehicle. Cells were then imaged live (unless otherwise indicated) in complete medium. Lysosome were scored as tubules if their length was greater than 4 µm.

Antigen presentation assays

For presentation of E$\alpha_{52–68}$ peptide, C57BL/6 mice with I-A^{b} background were used to isolate monocytes for BMDC differentiation, and C3H/HeN mice with I-A^{k} background (Charles River Canada, Kingston, ON) were used for presentation of Hen-egg lysozyme (HEL). Immature BMDCs were plated on Poly-D-lysine coated glass coverslips prior to incubation with model antigens. On day 7 of differentiation, dendritic cells were incubated with 2 mg/mL of HEL (Sigma-Aldrich) or 60 µM E$\alpha_{52–68}$ peptide (MyBioSource, San Diego, CA) in the presence or absence of inhibitors and/or LPS, for the time points indicated.

For surface detection of I-A^{k}::HEL$^{46–62}$ complexes, Aw3.18.14 mAb was isolated from the supernatant of hybridoma B-lymphocytes (ATCC, Manassas, VA). Briefly, cells were washed with ice-cold PBS 3 times, and incubated in ice-cold Aw3.18.14 for 30 minutes, then washed with PBS and fixed in 4% PFA for 30 minutes on ice. Following, cells were incubated in Dylight-conjugated donkey polyclonal antibody against mouse (1:500; Bethyl), in standard blocking buffer for 1 hr. For presentation of I-A^{b}::E$\alpha_{52–68}$ complexes, cells were washed 3 times with PBS and fixed in 4% PFA for 20 mins at RT. After, cells were permeabilized in 0.1% saponin in standard blocking buffer for 1 h. Following, cells were incubated in 1:75 mAb YAe (Santa Cruz Biotechnology, Dallas, Tx) in blocking buffer for 1 hour at RT, washed with PBS and then incubated Dylight-conjugated donkey polyclonal antibodies against mouse (1:500; Bethyl), in standard blocking

buffer for 1 hr. Antigen presentation of both I-A^k::$HEL^{46–61}$ and I-A^b::$E\alpha^{52–68}$ complexes was visualized using confocal microscopy.

Immunofluorescence and Fluorescence Microscopy

To fix and preserve lysosome tubules in RAW cells, cells were incubated with 0.45% (v/v) glutaraldehyde and 0.5% PFA (v/v) in PBS for 15 minutes at room temperature. Cells were then washed with PBS 4x, followed by incubation with 1 mg/mL ice-cold sodium borohydride (Sigma-Aldrich) for 5 min 3x to abate unreacted glutaraldehyde and quench its autofluorescence.

To visualize endogenous TFEB and TFE3, cells were fixed using 4% PFA for 15 min following treatment conditions. Cells were then treated with treated with 100 mM glycine in PBS to quench PFA, then in permeabilization buffer (0.2% Triton-X, 2% BSA in PBS) for 10 min and then blocked for 1 h in 2% BSA. Cells were incubated with rabbit anti-TFEB (1:200; Bethyl Laboratories, Montgomery, TX) or rabbit anti-TFE3 (1:500; Sigma-Aldrich) antibodies for 1 h, followed by Dylight-conjugated donkey polyclonal antibodies against rabbit (1:500; Bethyl) for 1 h. Nuclei were counter stained with 0.4 μg/mL of DAPI. For staining LAMP1, dextran-loaded cells were fixed in 0.45% (v/v) glutaraldehyde and 0.5% PFA (v/v) in PBS for 15 minutes at room temperature. Cells were washed with PBS 3x and quenched in 25mM glycine for 15 mins at room temperature. Cells were permeabilized in ice-cold methanol for 3 minutes and blocked in 2% BSA for 1 h. Cells were then incubated in primary rat anti-LAMP1 (1:100; Developmental Studies Hybridoma Bank) and secondary Dylight-conjugated donkey polyclonal antibodies against rat (1:500; Bethyl) for 1 h each. Cells were then mounted on a slide using DAKO mounting medium.

Live-cell imaging was done at 5% CO_2 and 37 °C using environmental control chambers. Live-cell and fixed-cell imaging was done with a Quorum Diskovery spinning disc confocal microscope system equipped with a Leica DMi8 microscope connected to an Andor Zyla 4.2 Megapixel sCMOS or an iXON 897 EMCCD camera, and controlled by Quorum Wave FX powered by MetaMorph software (Quorum Technologies, Guelph, ON). We also used an Olympus IX81 inverted microscope equipped with a Hamamatsu C9100-13 EMCCD camera and controlled with Volocity 6.3.0 (PerkinElmer). For super-resolution imaging, we employed the Zeiss Elyra PS1 imaging system equipped with an Axio Observer Z1 microscope fitted with the Andor iXon3 885 detector for structure illumination microscopy (SIM) and powered by Zeiss Zen 2012 software (Zeiss Microscopy, Jena, Germany). Super-resolution image acquisition was acquired by grating

for 3 rotations and 5 phases. All SIM reconstructed imaging was done using default settings for image reconstruction; to avoid artifact formation, only images with peak/mean ratios above 20 and noise filter less then -4 were accepted. After reconstruction, Volocity 6.3.0 (PerkinElmer) image analysis software was used. All microscopes were equipped with standard filters appropriate to fluorophores employed in this study, optics and stage automation.

Image analysis and volumetrics

The nuclear-to-cytosolic ratio of TFEB and TFE3 was estimated as the ratio of the mean fluorescence intensity in the nucleus over the mean intensity in the cytosol after background correction using ImageJ (v. 1.47 bundled with 64-bit Java). For Lamp1 and dextran colocalization, we used Mander's colocalization analysis to measure the degree of dextran colocalizing in LAMP1 structures, using the JACoP plugin in ImageJ after applying background subtraction. For volumetric analysis, we acquired confocal slices over 0.4 μm z-intervals. Due to technical limitations with SIM super-resolution imaging, we sampled the area of fluorescently labeled lysosomes by acquiring 3 confocal slices in the mid-point of the cell, where we quantified the pixel area for each slice and reported an average per cell. We then used Volocity 6.3.0 image analysis software to quantify the average number of fluorescent voxels or pixels within each cell. Due to the variation in lysosomal size from experiment to experiment we normalized the average voxel or pixel count to the corresponding control group. For lysosomal tubulation, we scored cells as positive for lysosome tubules if they displayed more than four lysosomal tubules greater than 4 μm. For antigen presentation analysis, we acquired confocal slices over 0.3 μm z-intervals and used Volocity to determine the total fluorescence intensity of antigen-MHCII complexes for 50-100 cells per experiment. To control for background, we established a threshold fluorescence intensity measure using a no-antigen control group for during each experiment. Image manipulation was done with ImageJ or Adobe Photoshop (Adobe Systems, San Jose, CA), without altering the relative signals within images or how data may be interpreted. All figures were assembled using Adobe Illustrator (Adobe Systems).

Puromycylation and Western blotting

For puromycylation assays, cells were treated with 10 μg/mL of puromycin (Sigma-Aldrich), or an equivalent water volume for the non-puromycin group, for the last 15 min of each treatment.

For all western blot analysis, cells were lysed in Laemmli buffer supplemented with 1:100 protease inhibitor cocktail (Sigma-Aldrich) and PhosSTOP protease inhibitor (Roche, Mississauga, ON) following each treatment. Proteins were then separated in a 10% or 15% SDS-PAGE, for high and low molecular weight proteins, respectively. Proteins were transferred to a polyvinylidene difluoride (PVDF) membrane (EMD Millipore, Toronto, ON), and blocked in 5% skim milk or BSA, in Tris-buffered saline buffer with 0.1% Tween 20 (TBST). Membranes were then immunoblotted using the appropriate primary and secondary antibodies prepared in 5% skim milk or BSA in TBST at the indicated dilutions. The primary antibodies used were rabbit anti-cathepsin D, ATP6V1H, ATP6V1D (GeneTex Inc., Irvine, CA), S6 ribosomal protein, phospho$^{Ser240/244}$- S6 ribosomal protein, p70 S6 kinase, phospho^{Thr389}-p70 S6 kinase, 4E-BP1, phospho$^{Thr37/46}$-4E-BP, β-actin, Ha-Tag and Tata-box binding protein (TBP; Cell Signaling Technologies, Danvers, MA), all at 1:1,000. We also used mouse anti-puromycin clone 12D10 (1:1000, EMD Millipore), rat anti-LAMP1 (1:200; Developmental Studies Hybridoma Bank, Iowa City, IO) and secondary HRP-linked antibodies raised in donkey (1:10,000, Bethyl). Proteins were detected using Clarity enhanced chemiluminescence (Bio-Rad Laboratories, Mississauga, ON) with a ChemiDoc XRS+ or ChemiDoc Touch imaging system (Bio-Rad). Protein quantification was performed using Image Lab software (Bio-Rad), where protein loading was normalized to levels of Tata box binding protein (TBP) or β-actin, and then normalized against the vehicle group.

Quantitative RT-PCR

For RT-qPCR analysis in BMDMs, total RNA was extracted using the GeneJET RNA purification kit (ThermoFisher). Following RNA isolation, equal quantities of mRNA were reverse transcribed with iScript Reverse Transcription Super Mix (Bio-Rad) following manufacturer's guidelines. The subsequent cDNA was amplified for quantitative PCR using the TaqMan Fast Advanced Master Mix (ThermoFisher) with appropriate TaqMan assays. The CFX96 Touch Real-Time PCR Detection System (Bio-Rad) and CFX Manager Software (Bio-Rad) were used for amplification and analysis. The TaqMan gene expression assays (ThermoFisher) for the reference genes Abt1 (Mm00803824_m1), B2M (Mm00437762_m1) and for target genes Atp6v1h (Mm00505548_m1), Atp6v1d (Mm00445832_m1), Lamp1 (Mm00495262_m1), Mcoln1 (Mm00522550_m1) and IL-6 (Mm00446190_m1) were done in triplicate. Target gene expression

was determined by relative quantification (ΔΔCt method) to Abt1 and the vehicle-treated control sample.

Polysome profiling

Polysome profiling was performed as detailed in Gandin *et al*. [66]. RAW264.7 cells were seeded in a 15-cm Petri dish and treated for 2 h or 6 h with a vehicle (DMSO), 500 ng/mL LPS from *Salmonella enterica* serotype minnesota Re 595, 100 nM torin1 for 2 h only, or the combination of LPS (500 ng/mL) and torin1 (100 nM) whereby cells were pre-treated for 15 minutes with torin1 before stimulation with LPS. Cells were harvested at 80% confluency, washed twice with ice-cold PBS containing 100 µg/mL cycloheximide and then lysed in hypotonic lysis buffer (5 mM Tris HCl, pH 7.5, 2.5 mM $MgCl_2$, 1.5 mM KCl, 100 µg/ml cycloheximide, 2 mM dithiothreitol (DTT), 0.5% Triton, and 0.5% sodium deoxycholate). Optical density values at 260 nm (OD_{260}) were measured in each lysate and 15 OD_{260} were then loaded on 5–50% sucrose gradients generated using Gradient Master (Biocomp, Fredericton, New Brunswick). Ten percent of lysates were saved as input samples for total RNA extraction. Sucrose gradients were subjected to ultracentrifugation (SW41 Ti 11E1698 rotor; Beckman at 260,000xg for 2 h at 4 °C) and fractionated by displacement using 60% sucrose/0.01% bromophenol blue on an ISCO Foxy fraction collector (35 s for each fraction, or ~ 750 µL per fraction) equipped with an ultraviolet lamp for continuous absorbance monitoring at 254 nm. Fractions were flash-frozen immediately after fractionation and stored at −80 °C. RNA was isolated with Trizol (Thermofisher) as per manufacturer's instruction. All experiments were carried out at least three independent biological replicates (n=3).

Reverse transcription and RT-qPCR were performed with iScript Reverse Transcription Super Mix (Bio-Rad) and TaqMan Fast Advanced Master Mix (ThermoFisher), respectively. All experiments were carried out at least three independent biological replicates (n=3). Analyses were carried out using relative standard curve method as instructed by the manufacturer. The following TaqMan assays were done using the primers described above for quantitative RT-PCR and in addition to Actb (Mm02619580_g1) and Ppia (Mm02342430_g1).

Acknowledgments

We would like to thank Dr. Rosa Puertollano at the NIH for her kind donation of the CRISPR-

deleted RAW strains (*tfeb*$^{-/-}$, *tfe3*$^{-/-}$ and *tfeb*$^{-/-}$ *tfe3*$^{-/}$ cells). We would like to thank Paul Paroutis and Michael Woodside from the Hospital for Sick Children Imaging Facility (Toronto, ON), and Christopher Spring from St. Michael's Hospital Flow Cytometry Facility (Toronto, ON), for their technical advice and expertise. We would like to thank the technical support staff at the Vivarium Facilities at St. Michael's Hospital for assistance in training and mice maintenance. The LAMP1 hybridoma antibody, developed by J.T. August, was obtained from the Developmental Studies Hybridoma Bank, created by the NICHD of the NIH and maintained at The University of Iowa, Department of Biology, Iowa City, IA.

Funding

This project and related work in the lab of R.J.B. was funded by an Operating Grant from the Canadian Institutes of Health Research, the Canada Research Chair Program, an Early Researcher Award from the Government of Ontario, and Ryerson University. V.E.B.H. was supported by Ontario Graduate Scholarships, Canada Graduate Scholarship and Ryerson Graduate Fellowship. J.A.D was funded by the NSERC undergraduate summer research award. I.T. is a Junior 2 Research Scholar of the Fonds de Recherche du Québec – Santé (FRQ-S) and the work in his lab related to this project was supported by Canadian Institutes of Health Research (PJT-148603).

References

1. Chan, Y.-H. M., Reyes, L., Sohail, S. M., Tran, N. K. & Marshall, W. F. Organelle Size Scaling of the Budding Yeast Vacuole by Relative Growth and Inheritance. *Curr. Biol.* **26,** 1221–1228 (2016).
2. Mullins, C. & Bonifacino, J. S. The molecular machinery for lysosome biogenesis. *BioEssays* **23,** 333–343 (2001).
3. Behnia, R. & Munro, S. Organelle identity and the signposts for membrane traffic. *Nature* **438,** 597–604 (2005).
4. Levy, D. L. & Heald, R. Mechanisms of Intracellular Scaling. *Annu. Rev. Cell Dev. Biol.* **28,** 113–135 (2012).
5. Mills, J. C. & Taghert, P. H. Scaling factors: Transcription factors regulating subcellular

domains. *BioEssays* **34,** 10–16 (2012).

6. Porta, C., Riboldi, E., Ippolito, A. & Sica, A. Molecular and epigenetic basis of macrophage polarized activation. *Seminars in Immunology* **27,** 237–248 (2015).
7. Trombetta, E. S., Ebersold, M., Garrett, W., Pypaert, M. & Mellman, I. Activation of lysosomal function during dendritic cell maturation. *Science (80-.).* **299,** 1400–1403 (2003).
8. Kelly, B. & O'Neill, L. A. J. Metabolic reprogramming in macrophages and dendritic cells in innate immunity. *Cell Res.* **25,** 771–84 (2015).
9. Janssens, S., Pulendran, B. & Lambrecht, B. N. Emerging functions of the unfolded protein response in immunity. *Nat. Immunol.* **15,** 910–919 (2014).
10. Hipolito, V. E. B., Ospina-Escobar, E. & Botelho, R. J. Lysosome remodelling and adaptation during phagocyte activation. *Cell. Microbiol.* **20,** e12824 (2018).
11. Delamarre, L., Pack, M., Chang, H., Mellman, I. & Trombetta, E. S. Differential lysosomal proteolysis in antigen-presenting cells determines antigen fate. *Science* **307,** 1630–4 (2005).
12. Gray, M. A. *et al.* Phagocytosis Enhances Lysosomal and Bactericidal Properties by Activating the Transcription Factor TFEB. *Curr. Biol.* **26,** 1955–1964 (2016).
13. Mrakovic, A., Kay, J. G., Furuya, W., Brumell, J. H. & Botelho, R. J. Rab7 and Arl8 GTPases are Necessary for Lysosome Tubulation in Macrophages. *Traffic* **13,** 1667–1679 (2012).
14. Vyas, J. M. *et al.* Tubulation of class II MHC compartments is microtubule dependent and involves multiple endolysosomal membrane proteins in primary dendritic cells. *J. Immunol.* **178,** 7199–210 (2007).
15. Saric, A. *et al.* mTOR controls lysosome tubulation and antigen presentation in macrophages and dendritic cells. *Mol. Biol. Cell* **27,** 321–333 (2016).
16. Hollenbeck, P. J. & Swanson, J. A. Radial extension of macrophage tubular lysosomes supported by kinesin. *Nature* **346,** 864–866 (1990).
17. Li, X. *et al.* A molecular mechanism to regulate lysosome motility for lysosome positioning and tubulation. *Nat. Cell Biol.* **18,** 404–17 (2016).
18. Swanson, J., Burke, E. & Silverstein, S. C. Tubular lysosomes accompany stimulated pinocytosis in macrophages. *J. Cell Biol.* **104,** 1217–1222 (1987).

19. Chow, A., Toomre, D., Garrett, W. & Mellman, I. Dendritic cell maturation triggers retrograde MHC class II transport from lysosomes to the plasma membrane. *Nature* **418,** 988–94 (2002).
20. Boes, M. *et al.* T-cell engagement of dendritic cells rapidly rearranges MHC class II transport. *Nature* **418,** 983–8 (2002).
21. Nakamura, N. *et al.* Endosomes are specialized platforms for bacterial sensing and NOD2 signalling. *Nature* **509,** 240–4 (2014).
22. Mantegazza, A. R. *et al.* TLR-dependent phagosome tubulation in dendritic cells promotes phagosome cross-talk to optimize MHC-II antigen presentation. *Proc. Natl. Acad. Sci. U. S. A.* **111,** 15508–13 (2014).
23. Mony, V. K., Benjamin, S. & O'Rourke, E. J. A lysosome-centered view of nutrient homeostasis. *Autophagy* **12,** 619–631 (2016).
24. Jewell, J. L., Russell, R. C. & Guan, K.-L. Amino acid signalling upstream of mTOR. *Nat. Rev. Mol. Cell Biol.* **14,** 133–9 (2013).
25. Lim, C. Y. & Zoncu, R. The lysosome as a command-and-control center for cellular metabolism. *J. Cell Biol.* **214,** 653–664 (2016).
26. Sancak, Y. *et al.* Ragulator-rag complex targets mTORC1 to the lysosomal surface and is necessary for its activation by amino acids. *Cell* **141,** 290–303 (2010).
27. Zoncu, R. *et al.* mTORC1 senses lysosomal amino acids through an inside-out mechanism that requires the vacuolar H+-ATPase. *Science (80-.).* **334,** 678–683 (2011).
28. Efeyan, A., Zoncu, R. & Sabatini, D. M. Amino acids and mTORC1: From lysosomes to disease. *Trends in Molecular Medicine* **18,** 524–533 (2012).
29. Martina, J. A. & Puertollano, R. Rag GTPases mediate amino acid-dependent recruitment of TFEB and MITF to lysosomes. *J. Cell Biol.* **200,** 475–491 (2013).
30. Bar-Peled, L., Schweitzer, L. D., Zoncu, R. & Sabatini, D. M. Ragulator is a GEF for the rag GTPases that signal amino acid levels to mTORC1. *Cell* **150,** 1196–1208 (2012).
31. Zhang, C. S. *et al.* The lysosomal v-ATPase-ragulator complex is a common activator for AMPK and mTORC1, acting as a switch between catabolism and anabolism. *Cell Metab.* **20,** 526–540 (2014).
32. Zoncu, R., Efeyan, A. & Sabatini, D. M. MTOR: From growth signal integration to cancer, diabetes and ageing. *Nature Reviews Molecular Cell Biology* **12,** 21–35 (2011).

33. Thoreen, C. C. The molecular basis of mTORC1-regulated translation. *Biochem. Soc. Trans.* **45,** 213–221 (2017).

34. Buszczak, M., Signer, R. A. J. & Morrison, S. J. Cellular differences in protein synthesis regulate tissue homeostasis. *Cell* **159,** 242–251 (2014).

35. Magnuson, B., Ekim, B. & Fingar, D. C. Regulation and function of ribosomal protein S6 kinase (S6K) within mTOR signalling networks. *Biochem. J.* **441,** 1–21 (2012).

36. Roux, P. P. & Topisirovic, I. Signaling pathways involved in the regulation of mRNA translation. *Mol. Cell. Biol.* **38,** MCB.00070-18 (2018).

37. Holz, M. K., Ballif, B. A., Gygi, S. P. & Blenis, J. mTOR and S6K1 mediate assembly of the translation preinitiation complex through dynamic protein interchange and ordered phosphorylation events. *Cell* **123,** 569–580 (2005).

38. Burnett, P. E., Barrow, R. K., Cohen, N. A., Snyder, S. H. & Sabatini, D. M. RAFT1 phosphorylation of the translational regulators p70 S6 kinase and 4E-BP1. *Proc. Natl. Acad. Sci. U. S. A.* **95,** 1432–7 (1998).

39. Beretta, L., Gingras, A. C., Svitkin, Y. V, Hall, M. N. & Sonenberg, N. Rapamycin blocks the phosphorylation of 4E-BP1 and inhibits cap-dependent initiation of translation. *EMBO J.* **15,** 658–64 (1996).

40. Jung, C. H. *et al.* ULK-Atg13-FIP200 Complexes Mediate mTOR Signaling to the Autophagy Machinery. *Mol. Biol. Cell* **20,** 1992–2003 (2009).

41. Ganley, I. G. *et al.* ULK1·ATG13·FIP200 complex mediates mTOR signaling and is essential for autophagy. *J. Biol. Chem.* **284,** 12297–12305 (2009).

42. Settembre, C. *et al.* A lysosome-to-nucleus signalling mechanism senses and regulates the lysosome via mTOR and TFEB. *Eur. Mol. Biol. Organ. J.* **31,** 1095–108 (2012).

43. Roczniak-Ferguson, A. *et al.* The transcription factor TFEB links mTORC1 signaling to transcriptional control of lysosome homeostasis. *Sci. Signal.* **5,** ra42 (2012).

44. Owen, K. A., Meyer, C. B., Bouton, A. H. & Casanova, J. E. Activation of Focal Adhesion Kinase by Salmonella Suppresses Autophagy via an Akt/mTOR Signaling Pathway and Promotes Bacterial Survival in Macrophages. *PLoS Pathog.* **10,** e1004159 (2014).

45. Moon, J.-S. *et al.* mTORC1-Induced HK1-Dependent Glycolysis Regulates NLRP3 Inflammasome Activation. *Cell Rep.* **12,** 102–115 (2015).

46. Long, F., Zhou, J. & Peng, H. Visualization and analysis of 3D microscopic images. *PLoS Comput. Biol.* **8,** e1002519 (2012).

47. Walter, T. *et al.* Visualization of image data from cells to organisms. *Nature Methods* **7,** S26–S41 (2010).

48. Gustafsson, M. G. L. Nonlinear structured-illumination microscopy: Wide-field fluorescence imaging with theoretically unlimited resolution. *Proc. Natl. Acad. Sci.* **102,** 13081–13086 (2005).

49. Barois, N., de Saint-Vis, B., Lebecque, S., Geuze, H. J. & Kleijmeer, M. J. MHC class II compartments in human dendritic cells undergo profound structural changes upon activation. *Traffic* **3,** 894–905 (2002).

50. Garrett, W. S. *et al.* Developmental control of endocytosis in dendritic cells by Cdc42. *Cell* **102,** 325–34 (2000).

51. Platt, C. D. *et al.* Mature dendritic cells use endocytic receptors to capture and present antigens. *Proc. Natl. Acad. Sci.* **107,** 4287–4292 (2010).

52. Drutman, S. B. & Trombetta, E. S. Dendritic cells continue to capture and present antigens after maturation in vivo. *J. Immunol.* **185,** 2140–6 (2010).

53. Kobayashi, T., Tanaka, T. & Toyama-Sorimachi, N. How do cells optimize luminal environments of endosomes/lysosomes for efficient inflammatory responses. *J. Biochem.* **154,** 491–499 (2013).

54. Swanson, J. a, Yirinec, B. D. & Silverstein, S. C. Phorbol esters and horseradish peroxidase stimulate pinocytosis and redirect the flow of pinocytosed fluid in macrophages. *J. Cell Biol.* **100,** 851–859 (1985).

55. Sardiello, M. *et al.* A Gene Network Regulating Lysosomal Biogenesis and Function. *Science (80-.).* **325,** 473–7 (2009).

56. Settembre, C., Fraldi, A., Medina, D. L. & Ballabio, A. Signals from the lysosome: a control centre for cellular clearance and energy metabolism. *Nat. Rev. Mol. Cell Biol.* **14,** 283–296 (2013).

57. Martina, J. A. *et al.* The nutrient-responsive transcription factor TFE3 promotes autophagy, lysosomal biogenesis, and clearance of cellular debris. *Sci. Signal.* **7,** ra9 (2014).

58. Polito, V. a *et al.* Selective clearance of aberrant tau proteins and rescue of neurotoxicity

by transcription factor EB. *EMBO Mol. Med.* **6,** 1–19 (2014).

59. Pastore, N. *et al.* TFEB and TFE3 cooperate in the regulation of the innate immune response in activated macrophages. *Autophagy* **12,** 1240–1258 (2016).
60. Raben, N. & Puertollano, R. TFEB and TFE3: Linking Lysosomes to Cellular Adaptation to Stress. *Annu. Rev. Cell Dev. Biol.* **32,** 255–278 (2016).
61. Liu, A. P., Botelho, R. J. & Antonescu, C. N. The big and intricate dreams of little organelles: Embracing complexity in the study of membrane traffic. *Traffic* (2017). doi:10.1111/tra.12497
62. Zhang, X. *et al.* MCOLN1 is a ROS sensor in lysosomes that regulates autophagy. *Nat. Commun.* **7,** 12109 (2016).
63. Schott, J. *et al.* Translational Regulation of Specific mRNAs Controls Feedback Inhibition and Survival during Macrophage Activation. *PLoS Genet.* **10,** e1004368 (2014).
64. Graczyk, D., White, R. J. & Ryan, K. M. Involvement of RNA Polymerase III in Immune Responses. *Mol. Cell. Biol.* **35,** 1848–1859 (2015).
65. Masvidal, L., Hulea, L., Furic, L., Topisirovic, I. & Larsson, O. mTOR-sensitive translation: Cleared fog reveals more trees. *RNA Biology* **14,** 1299–1305 (2017).
66. Gandin, V. *et al.* Polysome fractionation and analysis of mammalian translatomes on a genome-wide scale. *J. Vis. Exp.* (2014). doi:10.3791/51455
67. Piehler, A. P., Grimholt, R. M., Ovstebo, R. & Berg, J. P. Gene expression results in lipopolysaccharide-stimulated monocytes depend significantly on the choice of reference genes. *BMC Immunol.* **11,** 21 (2010).
68. Gordon, E. B. *et al.* Inhibiting the mammalian target of rapamycin blocks the development of experimental cerebral malaria. *MBio* **6,** e00725 (2015).
69. Rong, L. *et al.* Control of eIF4E cellular localization by eIF4E-binding proteins, 4E-BPs. *RNA* **14,** 1318–27 (2008).
70. Dadaglio, G., Nelson, C. A., Deck, M. B., Petzold, S. J. & Unanue, E. R. Characterization and quantitation of peptide-MHC complexes produced from hen egg lysozyme using a monoclonal antibody. *Immunity* **6,** 727–738 (1997).
71. Murphy, D. B. *et al.* Monoclonal antibody detection of a major self peptide. MHC class II complex. *J. Immunol.* **148,** 3483–3491 (1992).
72. Su, X. *et al.* Interferon-γ regulates cellular metabolism and mRNA translation to

potentiate macrophage activation. *Nat. Immunol.* **16,** 838–849 (2015).

73. Lelouard, H. *et al.* Regulation of translation is required for dendritic cell function and survival during activation. *J. Cell Biol.* **179,** 1427–39 (2007).
74. Piccirillo, C. A., Bjur, E., Topisirovic, I., Sonenberg, N. & Larsson, O. Translational control of immune responses: From transcripts to translatomes. *Nature Immunology* **15,** 503–511 (2014).
75. Boes, M. *et al.* T Cells Induce Extended Class II MHC Compartments in Dendritic Cells in a Toll-Like Receptor-Dependent Manner. *J. Immunol.* **171,** 4081–4088 (2003).
76. Thoreen, C. C. *et al.* A unifying model for mTORC1-mediated regulation of mRNA translation. *Nature* **485,** 109–13 (2012).
77. Nandagopal, N. & Roux, P. P. Regulation of global and specific mRNA translation by the mTOR signaling pathway. *Transl. (Austin, Tex.)* **3,** e983402 (2015).
78. Ma, X. M., Yoon, S.-O., Richardson, C. J., Jülich, K. & Blenis, J. SKAR Links Pre-mRNA Splicing to mTOR/S6K1-Mediated Enhanced Translation Efficiency of Spliced mRNAs. *Cell* **133,** 303–313 (2008).
79. Yuan, S. *et al.* Target-of-rapamycin complex 1 (Torc1) signaling modulates cilia size and function through protein synthesis regulation. *Proc. Natl. Acad. Sci. U. S. A.* **109,** 2021–6 (2012).
80. Gaard, E. *et al.* Horizontal and vertical copepod distribution and abundance on the Mid-Atlantic Ridge in June 2004. *Deep. Res. Part II Top. Stud. Oceanogr.* **55,** 59–71 (2008).
81. Meyuhas, O. Synthesis of the translational apparatus is regulated at the translational level. *Eur. J. Biochem.* **267,** 6321–30 (2000).
82. Thoreen, C. C. *et al.* A unifying model for mTORC1-mediated regulation of mRNA translation. *Nature* **485,** 109–113 (2012).
83. Hsieh, A. C. *et al.* The translational landscape of mTOR signalling steers cancer initiation and metastasis. *Nature* **485,** 55–61 (2012).
84. Bilanges, B. *et al.* Tuberous sclerosis complex proteins 1 and 2 control serum-dependent translation in a TOP-dependent and -independent manner. *Mol. Cell. Biol.* **27,** 5746–5764 (2007).
85. Gandin, V. *et al.* NanoCAGE reveals 5' UTR features that define specific modes of translation of functionally related MTOR-sensitive mRNAs. *Genome Res.* **26,** 636–648

(2016).

86. Larsson, O. *et al.* Distinct perturbation of the translatome by the antidiabetic drug metformin. *Proc. Natl. Acad. Sci.* **109,** 8977–8982 (2012).

87. Inaba, K. *et al.* Generation of large numbers of dendritic cells from mouse bone marrow cultures supplemented with granulocyte/macrophage colony-stimulating factor. *J. Exp. Med.* **176,** 1693–1702 (1992).

88. Weischenfeldt, J. & Porse, B. Bone Marrow-Derived Macrophages (BMM): Isolation and Applications. *Cold Spring Harb. Protoc.* **2008,** pdb.prot5080-pdb.prot5080 (2008).

Figure Legends

Figure 1: LPS-mediated activation of phagocytes augments lysosome volume. a. Lysosomes in bone-marrow derived macrophages (BMDMs), bone-marrow derived dendritic cells (BMDCs), and in RAW macrophages before and after 2 h of LPS stimulation, the latter causing extensive lysosome tubulation. Images were acquired by live-cell spinning disc confocal microscopy. Scale bar = 5 µm. **b.** Relative lysosome volume between counterpart resting and LPS-treated phagocytes acquired by live-cell spinning disc confocal imaging. **c.** Relative lysosome volume in fixed resting and LPS-treated RAW macrophages. **d.** Relative lysosome area from the mid-section of resting and LPS-activated phagocytes using images acquired by SIM-enacted super- resolution microscopy. All experiments were repeated at least three independent times. Data are based on 30-40 cells per condition per experiment and are shown as the mean ± standard error of the mean. Statistical analysis was done using one-way ANOVA and unpaired Student's t-test, where the asterisk * indicates a significant increase in lysosome volume relative to resting phagocytes ($p<0.05$).

Figure 2: Macrophage activation increases lysosomal holding capacity. a. Image compilation of 6 representative fields in false-colour showing changes in intensity of Lucifer yellow acquired by endocytosis over the indicated time in resting primary macrophages or macrophages stimulated with LPS. Scale = 250µm. Color scale: 0 – 4095 (low-high). **b**. Accumulation of Lucifer yellow continuously endocytosed over indicated timeframe in resting, activated with LPS for 2 h or co-

activated with LPS continuously. **c**. Rate of pinocytosis of Lucifer yellow in primary macrophages treated as indicated. **d**. Retention of Lucifer yellow in resting or LPS-treated primary macrophages after 0.5 h internalization and chase in probe-free medium over indicate times. In all cases, fluorescence measurements were acquired by fluorimeter plate-imager. Data are shown as the mean ± standard error of the mean from at least 3 independent experiments. Statistical analysis was done using an Analysis of Covariance, whereby controlling for time as a continuous variable. An asterisk indicates a significant increase in Lucifer yellow for that series relative to resting phagocytes ($p<0.05$).

Figure 3: Lysosome remodelling requires protein biosynthesis. **a**. Western blot analysis of whole cell lysates from resting primary macrophages or macrophages exposed to the indicated combinations and time of LPS and cycloheximide (CHX). **b**. Quantification of Western blots showing the levels of LAMP1, cathepsin D (CtsD) and the V-ATPase V_1 subunit H and D normalized to TBP. Data are shown as the mean ± standard error of the mean from at least 3 independent experiments. For A and B, "2/4" indicates cells stimulated with 2 h of LPS, followed by a 4 h chase, whereas 2 and 6 h represent cells continuously exposed to LPS for those time periods. **c.** Live-cell spinning disc confocal micrographs of pre-labelled lysosomes in resting primary macrophages or those stimulated with LPS and/or cycloheximide. Scale bar = 5 µm. **d.** Relative lysosome volume between resting primary macrophages and those exposed to specified conditions. Shown is the mean ± standard error of the mean from 30-40 cells for each condition and experiment, across at least 3 independent experiments. Statistical analysis was done with ANOVA and unpaired Student's t-test. The asterisk * indicates a significant difference ($p<0.05$).

Figure 4: Lysosome remodelling is independent of TFEB and TFE3 activation. **a**. TFEB and TFE3 subcellular localization in resting primary macrophages (vehicle) or those treated with LPS for 2 or 6 h, or with torin1. Green = TFEB or TFE3 immunofluorescence signal; white = nuclei stained with DAPI. Areas within dashed boxes are magnified as insets. **b**. Nuclear to cytosolic ratio of TFEB or TFE3 fluorescence intensity. Shown is the mean ± standard error of the mean from 30-40 cells per condition per experiment across at least 3 independent experiments. **c, d**. Relative mRNA levels of select lysosomal genes (c) or interleukin-6 (d) in activated primary macrophages relative to Abt1 housekeeping gene and normalized against resting cells.

Quantification was done with qRT-PCR by measuring the ΔΔCt as described in methods. Shown is the mean ± standard error of the mean from four independent experiments. **e.** Lysosomes in wild-type, *tfeb*$^{-/-}$, *tfe3*$^{-/-}$ and *tfeb*$^{-/-}$ *tfe3*$^{-/-}$ RAW strains before and after 2 h of LPS stimulation. Images were acquired by live-cell spinning disc confocal microscopy. Yellow arrowheads illustrate tubular lysosomes. **f.** Relative lysosome volume between LPS-treated and resting counterpart RAW strains acquired by live-cell spinning disc confocal imaging. Shown is the mean ± standard error of the mean from 30-40 cells per condition per experiment across three independent experiments. All statistical analysis was done with ANOVA and unpaired Student's t-test. The asterisk * indicates a significant difference relative to resting condition ($p<0.05$). For a and e, scale bar = 5 μm.

Figure 5: mTOR stimulates lysosome volume and holding capacity. a. Western blot analysis of whole cell lysates from resting and activated primary macrophages. Total levels and phosphorylation status of S6K and 4EBP1 were monitored using indicated antibodies. TBP served as a loading control. **b.** Normalized ratio of p-p70S6K and p-4EBP1 to total p70S6K and 4E-BP1 protein. Shown is the mean ± standard deviation from three independent blots. **c.** Lysosomes in primary macrophages were pre-treated with a vehicle (DMSO), Akti or torin1, followed by 2 h LPS stimulation where indicated. Images were acquired by live-cell spinning disc confocal microscopy. Scale bar = 5 μm. **d.** Lysosome volume in primary macrophages treated as indicated normalized to resting macrophages. Shown is the mean ± standard error of the mean from 30-40 cells per condition per experiment across three independent experiments. **e.** Quantification of pinocytic capacity in macrophages treated as indicated. Shown is the mean ± standard error of the mean from four independent experiments. For b and d, data was statistically analysed with ANOVA and unpaired Student's t-test (*$p<0.05$). For E, data was statistically assessed using an Analysis of Covariance, whereby controlling for time as a continuous variable. An asterisk indicates a significant increase in Lucifer yellow for that series relative to resting phagocytes (*$p<0.05$).

Figure 6: LPS stimulates global protein synthesis in primary macrophages. a. Western blot analysis of protein puromycylation in resting and activated primary macrophages. LPS increases the amount of puromycylation indicating a boost in global protein synthesis that is blocked by

mTOR inhibitors or cycloheximide. Lane 1 are control lysates from cells not exposed to puromycin. The band indicated by arrow is a non-specific band recognized by the anti-puromycin antibody. p-p70S6K and β-actin were used to monitor mTOR status and as a loading control, respectively. **b.** Normalized puromycylation signal (excluding non-specific band) normalized over β-actin signal. Data is shown as the mean ± standard deviation from four independent experiments. Statistical analysis was done with an ANOVA, where * indicates conditions that are statistically distinct from control (*$p<0.05$).

Figure 7: LPS increases translation of mRNAs encoding lysosomal proteins in an mTOR-dependent manner. a-f. Percent of target mRNA (a: LAMP1, b: ATP6V1H, c: ATP6V1D, d: β-actin, e: PPIA, and f: B2M) associated with each ribosome fraction in resting, LPS- or LPS/torin1-treated RAW cells. Left and middle panels show 2 h and 6 h treatments, respectively. Shown is a representative experiment (as the mean percentage ± standard error) from four independent experiments, each of which contained three technical replicates. Right panels: Pooled percent mRNA in subpolysomal (fractions 7-10), light polysosome (fractions 11 and 12) and heavy polysomes (fractions 13-16). Shown is the mean percent ± standard deviation from four independent experiments with each point in triplicate for each experiment and mRNA. Heavy fractions were statistically analysed by ANOVA and Tukey's post-hoc test, where * indicates statistical difference from resting conditions, while ** indicates differences between LPS and LPS+torin1 conditions within 2 and 6 h exposure.

Figure 8: S6 kinase is required for the LPS-mediated lysosome expansion. a. Lysosomes in primary macrophages were pre-treated with LY258470 (LY2) followed by 2 h LPS stimulation where indicated. Images were acquired by live-cell spinning disc confocal microscopy. Scale bar = 5 μm. **b.** Lysosomal tubulation was scored for each condition as shown, where a tubule was defined as longer than 4 μm in length. Tubulation index was determined by normalizing scores to resting cells. **c.** Total lysosome volume in primary macrophages treated as indicated. For **b** and **c,** shown are the mean ± standard error of the mean from 30-40 cells per condition per experiment, across three independent experiments. **d.** Western blot analysis of whole cell lysates from resting and activated primary macrophages with or without LY258470. **e.** Quantification of Western blots showing the levels of LAMP1 and the V-ATPase V_1 subunits H and D, normalized to β-actin.

pS6K and total S6K blots are shown to support effectiveness of LY258470 treatment. Shown is the mean ± standard deviation of the mean from five independent blots. For **b, c** and **e**, data was statistically analysed with ANOVA and unpaired Student's t-test (*p<0.05).

Figure 9: Active 4E-BP1 suppresses LPS-mediated lysosome expansion. a. Lysosomes in resting or LPS stimulated (2 h) RAW cells stably expressing the 4E-BP1 (4Ala) phosphorylation mutant or the empty pBabe vector. Images were acquired by live-cell spinning disc confocal microscopy. Scale bar = 10 μm. **b.** Lysosomal tubulation was scored for each, where a tubule was defined as longer than 4 μm in length. Tubulation index was determined by normalizing scores to resting. **c.** Total lysosome volume in engineered RAW macrophages treated as indicated. For **b** and **c,** shown are the mean ± standard error of the mean from 30-40 cells per condition per experiment, across three independent experiments. **d.** Western blot analysis of whole cell lysates from stable cell lines. **e.** Quantification of Western blots showing the levels of LAMP1 and the V-ATPase V_1 subunits H and D, normalized to β-actin for both cell lines. Anti-HA blot demonstrates expression of 4E-BP1^{4Ala}. Shown is the mean ± standard deviation of the mean from 3 independent blots. For **b, c** and **e**, data was statistically analysed with ANOVA and unpaired Student's t-test (*p<0.05).

Figure 10: mTOR and S6 kinase control E$\alpha_{52–68}$ peptide presentation in activated BMDCs. BMDCs were incubated with E$\alpha^{52–68}$ peptide for 4 or 6 hours in the presence or absence LPS with or without torin1 and LY258470. Cells were then fixed and stained with Y-Ae antibodies to detect I-A^b::E$\alpha^{52–68}$ complex formation and DAPI. **a**. I-A^b::E$\alpha^{52–68}$ complexes (displayed in pseudo-colour) and DAPI (grayscale) are shown for BMDCs treated as indicated. **b, c.** Anti-I-A^b::E$\alpha^{52–68}$ antibody signal was quantified by fluorescence intensity associated with each cell. Shown is the mean of the total fluorescence intensity of I-A^b::E$\alpha^{52–68}$ complexes ± standard deviation from three experiments, where 50-100 cells were quantified for each. Data was analysed using ANOVA, whereby * indicates a difference compared to stimulated BMDCs exposed to E$\alpha^{52–68}$ and ** indicates a difference compared to LPS-stimulated BMDCs fed E$\alpha^{52–68}$ (p<0.05). Scale bar = 30 μm. Color scale: 0 – 2500 (low-high). **Supp. Fig. S6c** show similar data for HEL presentation.

Supplemental Figure Legends

Supplemental Figure 1: Preservation of tubules during fixation and super-resolution imaging. a. RAW macrophage lysosomes labeled with fluid phase probes fluorescent probes, were imaged live or fixed with 4% PFA or mixture of PFA and glutaraldehyde as explained in methods. **b.** Percent lysosome tubulation was recorded within the population for cells exhibiting 4 or more lysosomal tubules longer then 4 μm. **c.** Wide field (WF) illumination or structured illumination microscopy (SIM) images of lysosomes in RAW macrophages, bone marrow derived macrophages (BMDM) and bone-marrow derived dendritic cells (BMDCs), before and after 2 h of LPS stimulation. Scale bar = 5 μm.

Supplemental Figure 2: Activated RAW macrophages have a larger lysosome holding capacity. a. Accumulation of Lucifer yellow (LY) in resting and activated RAW macrophages. RAW cells were stimulated and then allowed to internalize LY over time. **b**. Pinocytosis rate by quantifying uptake of Lucifer yellow in RAW macrophages treated as indicated. **c**. Retention of Lucifer yellow chased in probe-free medium in RAW cells previously treated as indicated and pre-labelled with Lucifer yellow for 1 h. In all cases, fluorescence measurements were done by flow cytometry. **d.** Pinocytosis in increasingly maturing DCs exposed to LPS. Microscopy was used to measure the uptake of fluorescent dextran for 30 min by DCs exposed to LPS over indicated time points. Shown is the mean ± standard error of the mean from at least three experiments. For statistical analysis, ANOVA or Analysis of Covariance was used, whereby an asterisk indicates a significant difference in fluorescent probe levels compared to resting (*$p<0.05$).

Supplemental Figure 3: Basal lysosome properties and trafficking is indistinguishable in wild-type RAWs and strains deleted for TFEB and/or TFE3. a. LAMP1 levels in whole cell lysates from wild-type and deletion mutants of TFEB and/or TFE3. **b**. Quantification of LAMP1 levels in knock-out cells. LAMP1 levels were normalized to β-actin to control for loading. Statistical analysis using ANOVA determined that LAMP1 levels did not vary across strains. **c**. Co-localization of dextran and LAMP1 in wild-type and deletion strains. Right, middle and left panels show dextran (red), endogenous LAMP1 (green) and merge, respectively. Scale bar = 5 μm. **d.** Mander's coefficient of dextran co-localizing in LAMP1 structures. Data shown as relative units (R.U), normalized to wild-type strain. **e.** Pinocytosis label after a 1 hr pulse and 1 hr chase

of fluorescent dextran in resting wild-type and deletion RAW strains, measured by microscopy and image analysis. Mean fluorescence intensity was normalized to wild-type strain and is represented as relative units (R.U). **f**. Dextran fluorescence in RAW and deletion strains 2 h after LPS exposure or vehicle. For all data, shown are the mean± standard deviation from at least three independent experiments.

Supplemental Figure 4: Polysome profiling of RAW macrophages: additional replicate data. Percent of target mRNA **(a:** LAMP1, **b**: ATP6V1H, **c**: ATP6V1D **d:** β-actin **e:** PPIA and **f.** B2M) associated with each ribosome fraction in resting, LPS-treated macrophages and macrophages co-exposed to LPS and torin1, or treated with torin1 alone. Left, middle and right panels show 2 h, 6 h and torin1 (2 h) treatments, respectively. Shown, is an additional biological replicate of the experiment described in Figure 7a-d.

Supplemental Figure 5: The effects of RAW macrophage stimulation by LPS on protein synthesis. a-d. Percent of target mRNA **(a:** LAMP1, **b**: ATP6V1H, **c**: ATP6V1D **d:** PPIA, **e**: β-actin and **f.** B2M) associated with each ribosome fraction in resting and torin1 (2 h; 100 nM) treated cells.

Supplemental Figure 6: S6K activity during LY258470 treatment and effect on HEL presentation by BMDCs. a. Normalized ratio of phosphorylated ribosomal S6 to total ribosomal S6 as depicted in Fig. 8d, in primary macrophages treated with LY258470 (LY2) alone, or co-incubated with LPS for 2 h. Shown is the mean ± standard deviation of the mean from five independent blots. **b.** Relative mRNA levels of select lysosomal genes (right) or interleukin-6 (left) in LPS and/or LY2 treated primary macrophages relative to Abt1 housekeeping gene and normalized against resting cells. Quantification was done with qRT-PCR by measuring the ΔΔCt as described in methods. Shown is the mean ± standard error of the mean from four independent experiments. **c**. I-A^k::HEL^{46-61} presentation in BMDCs after incubation with HEL for 6 hours in the presence and/or absence of LPS, torin1 and LY2. I-A^k::HEL^{46-61} cell surface levels were detected by staining unpermeabilized cells with the monoclonal antibody Aw3.18.14 **d.** Quantification of total average fluorescence intensity of I-A^k::HEL^{46-61} complexes at the plasma membrane. Shown is the mean ± standard deviation from three experiments, where 50-100 cells were quantified for each. Data was analysed using ANOVA, whereby * indicates a difference

compared to the Resting+HEL condition and ** indicates a difference compared to HEL+LPS ($p<0.05$). Scale bar = 15µm. Color scale: 0 – 12000 (low-high).

Figure 1

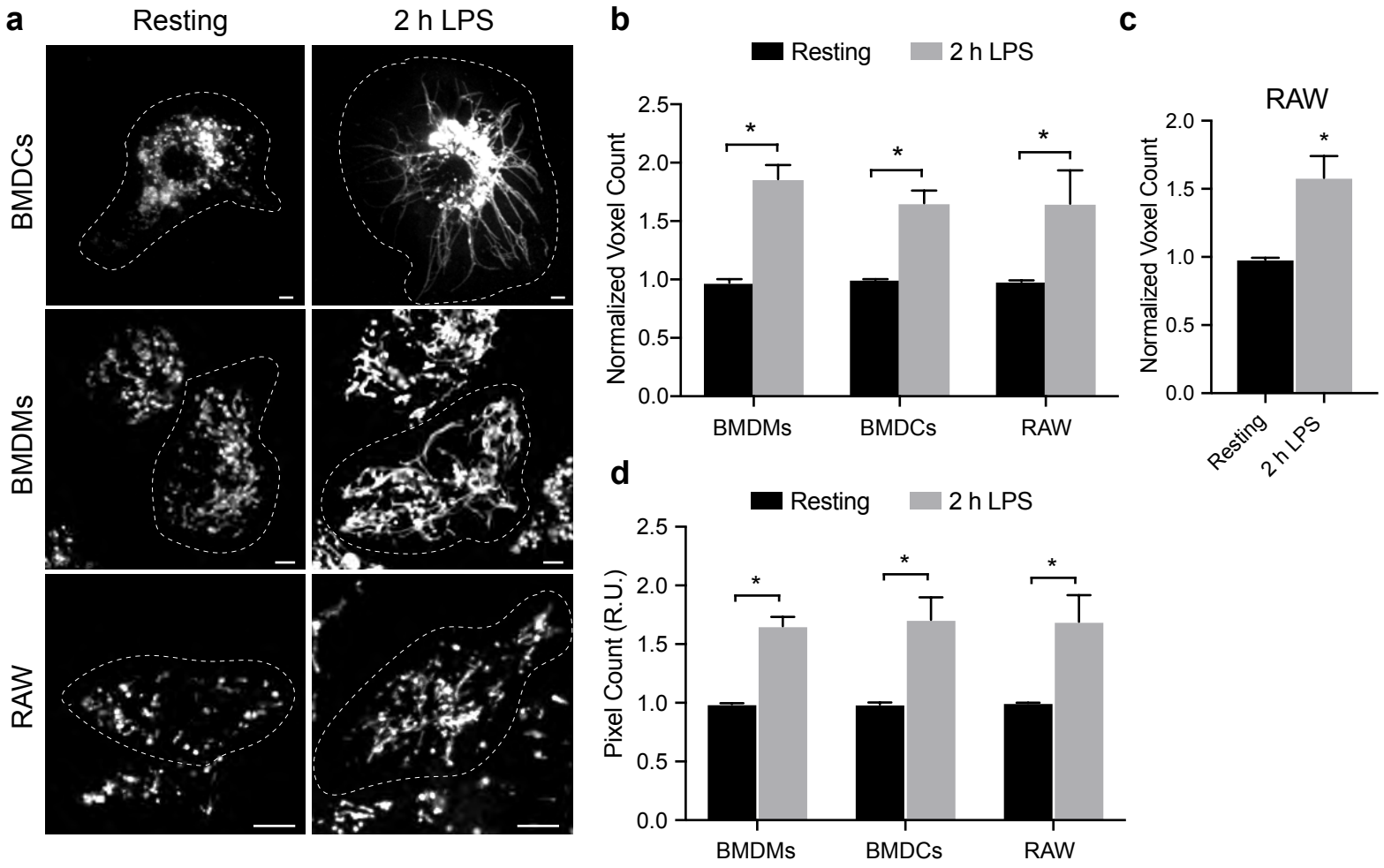

Figure 2

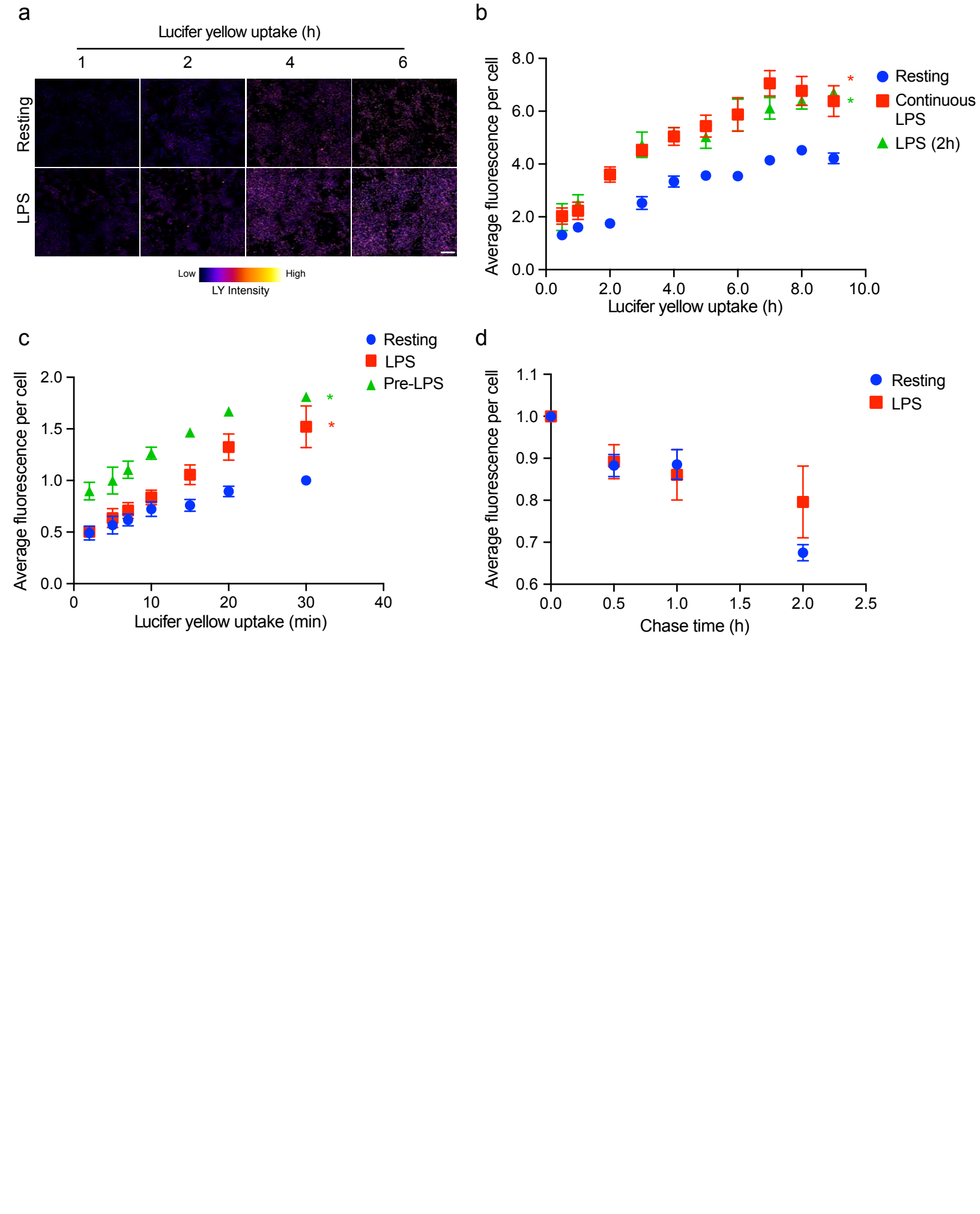

Figure 3

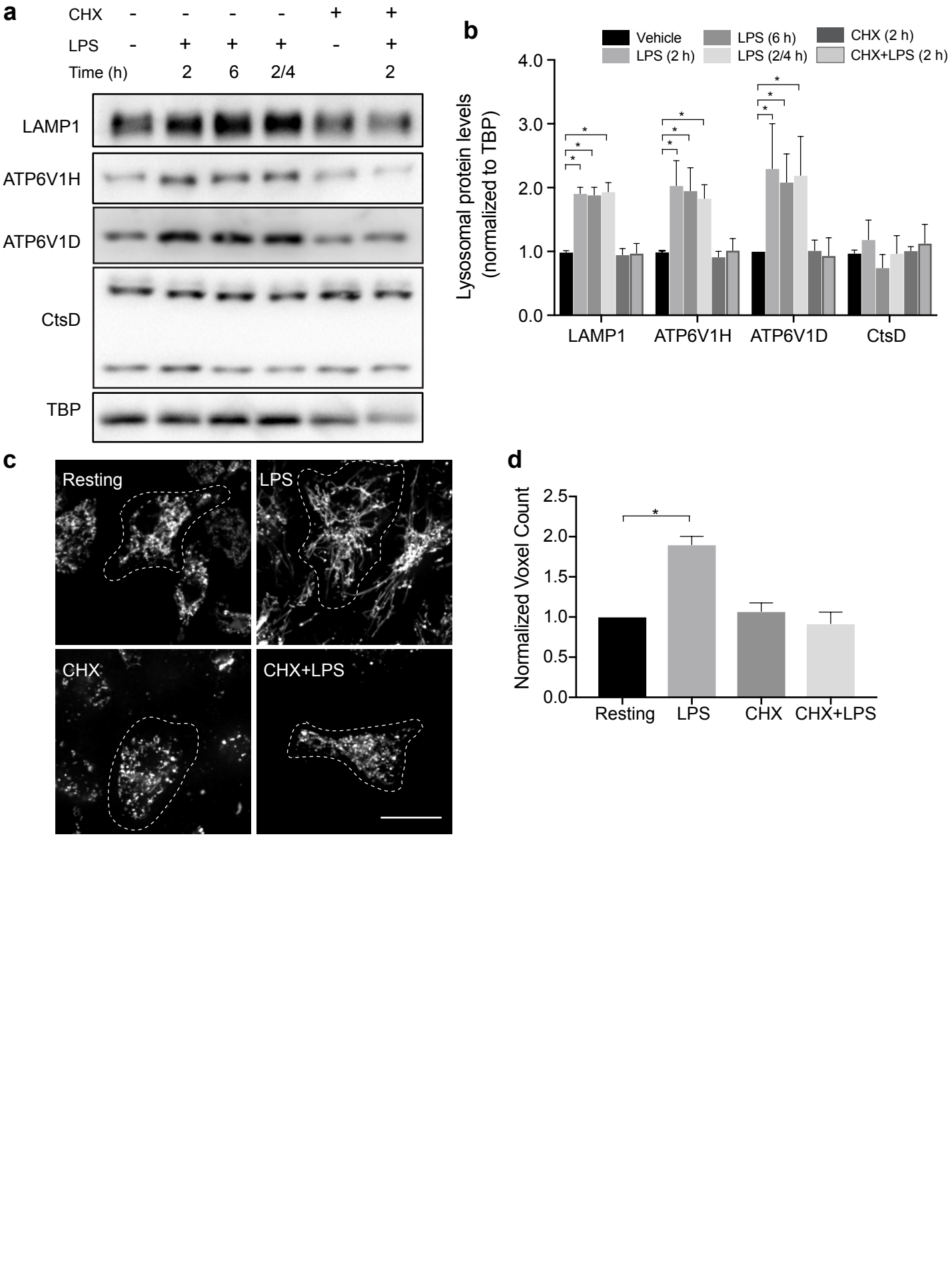

Figure 4

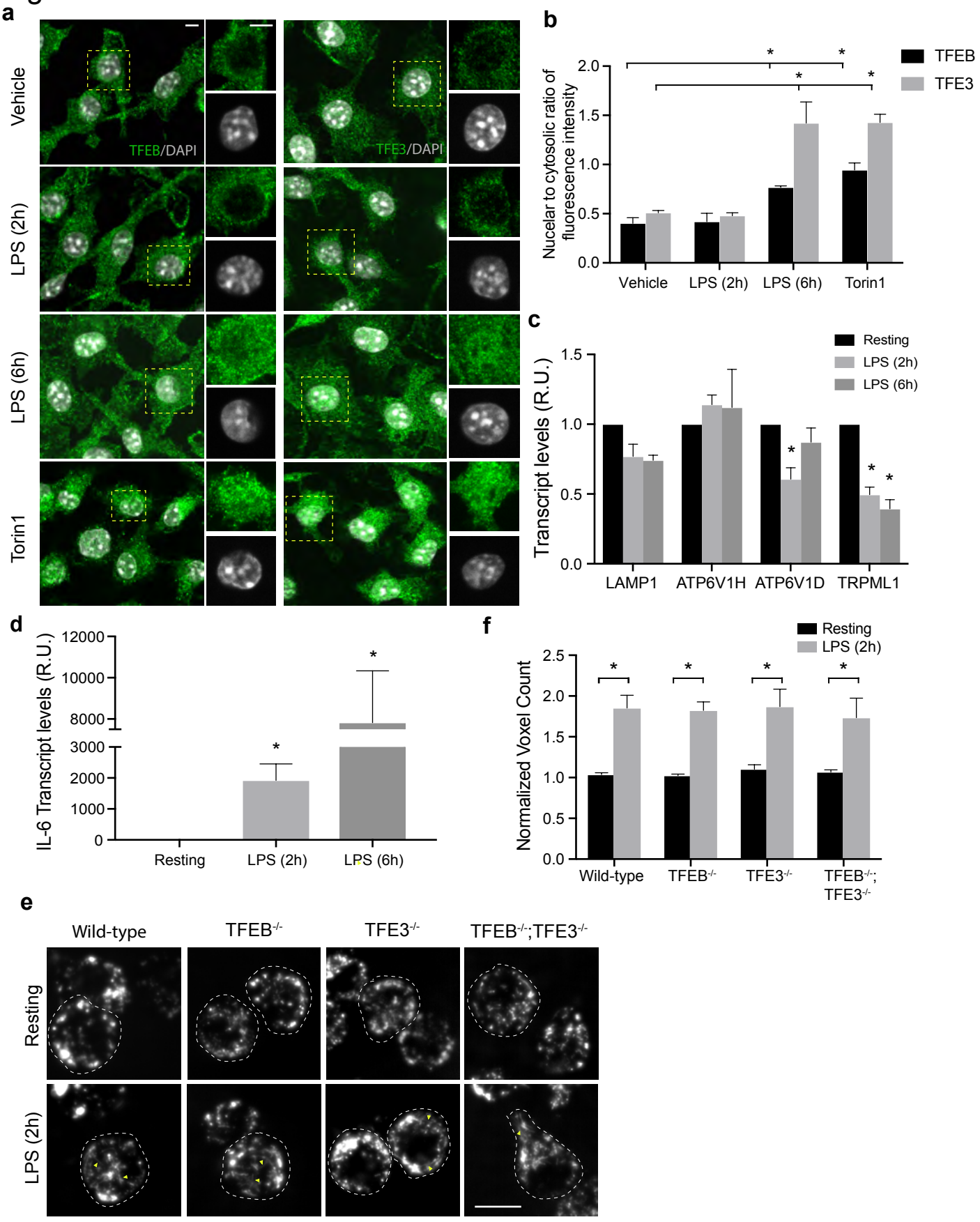

Figure 5

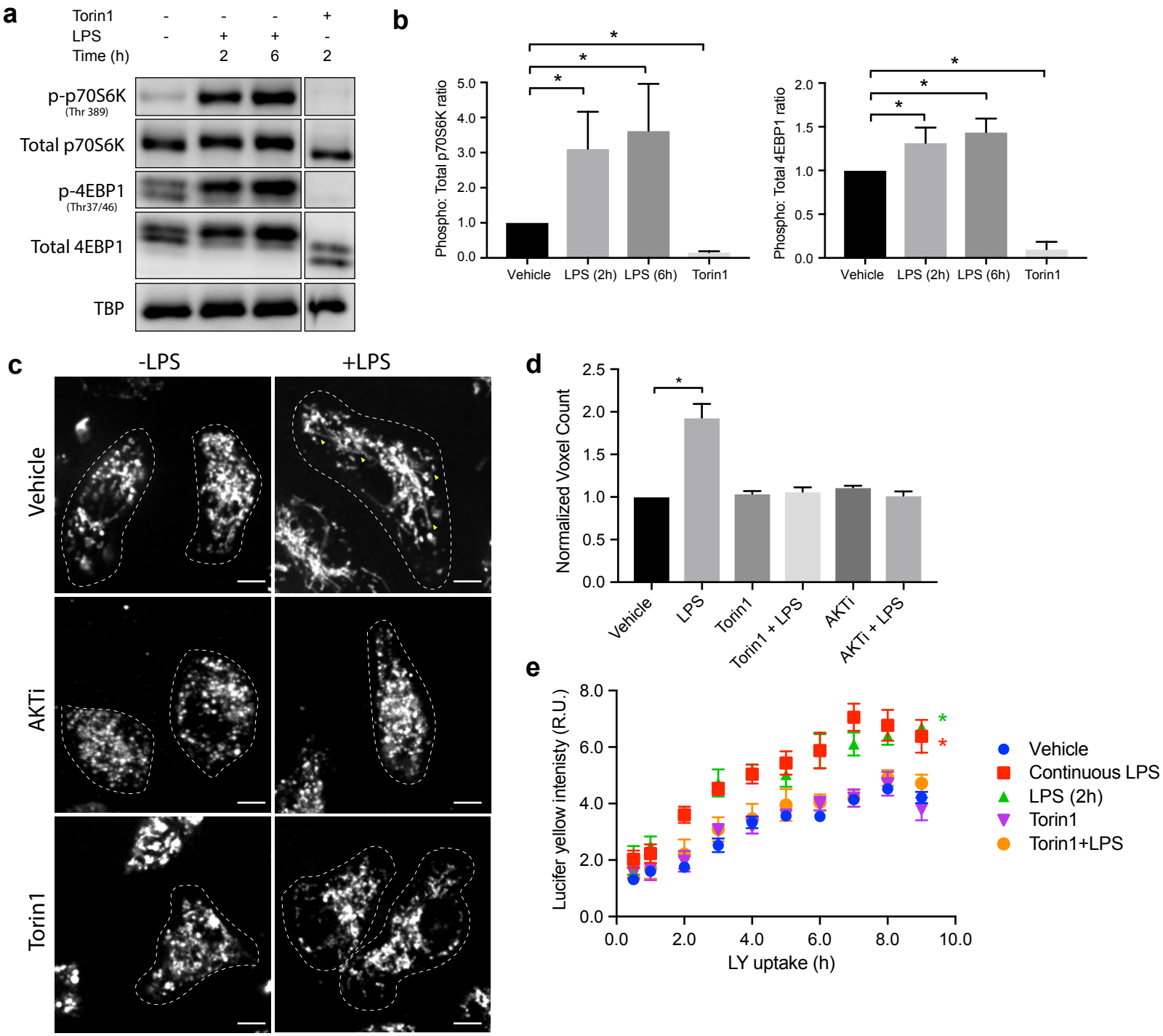

Figure 6

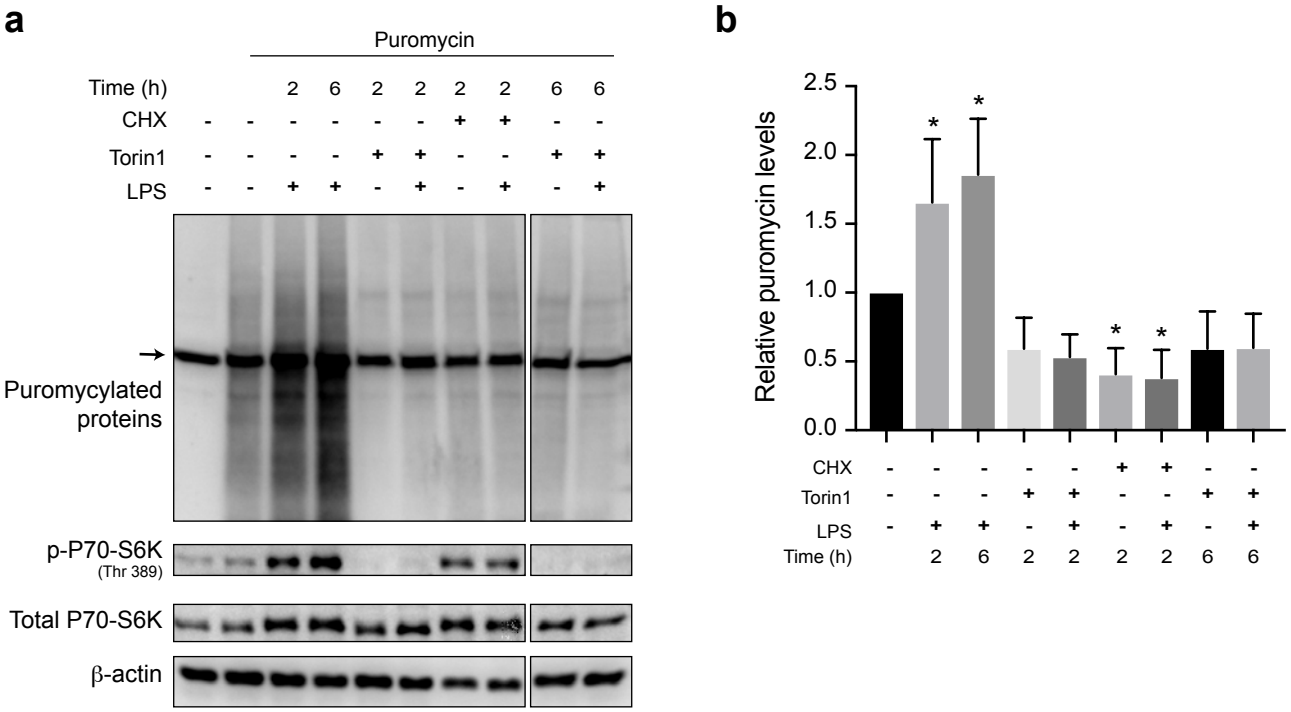

Figure 7

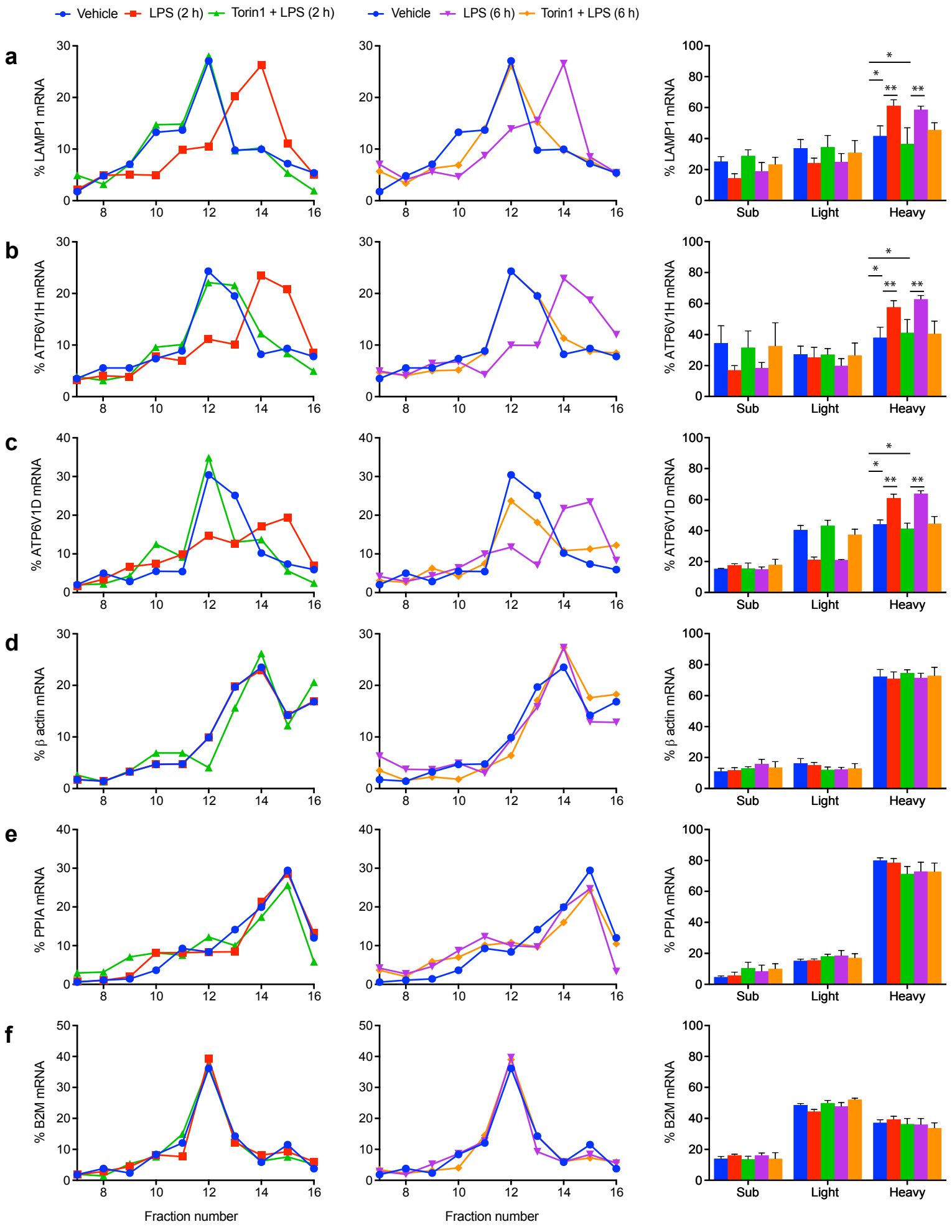

Figure 8

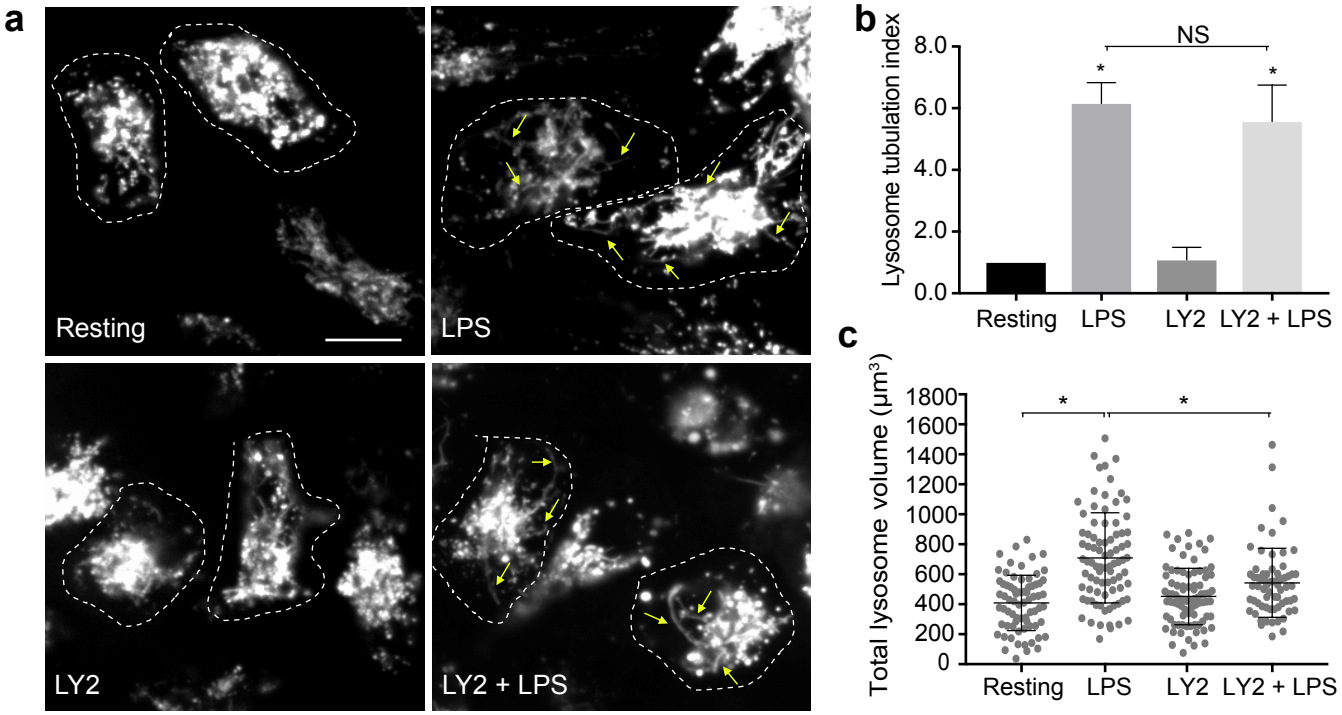

Figure 9

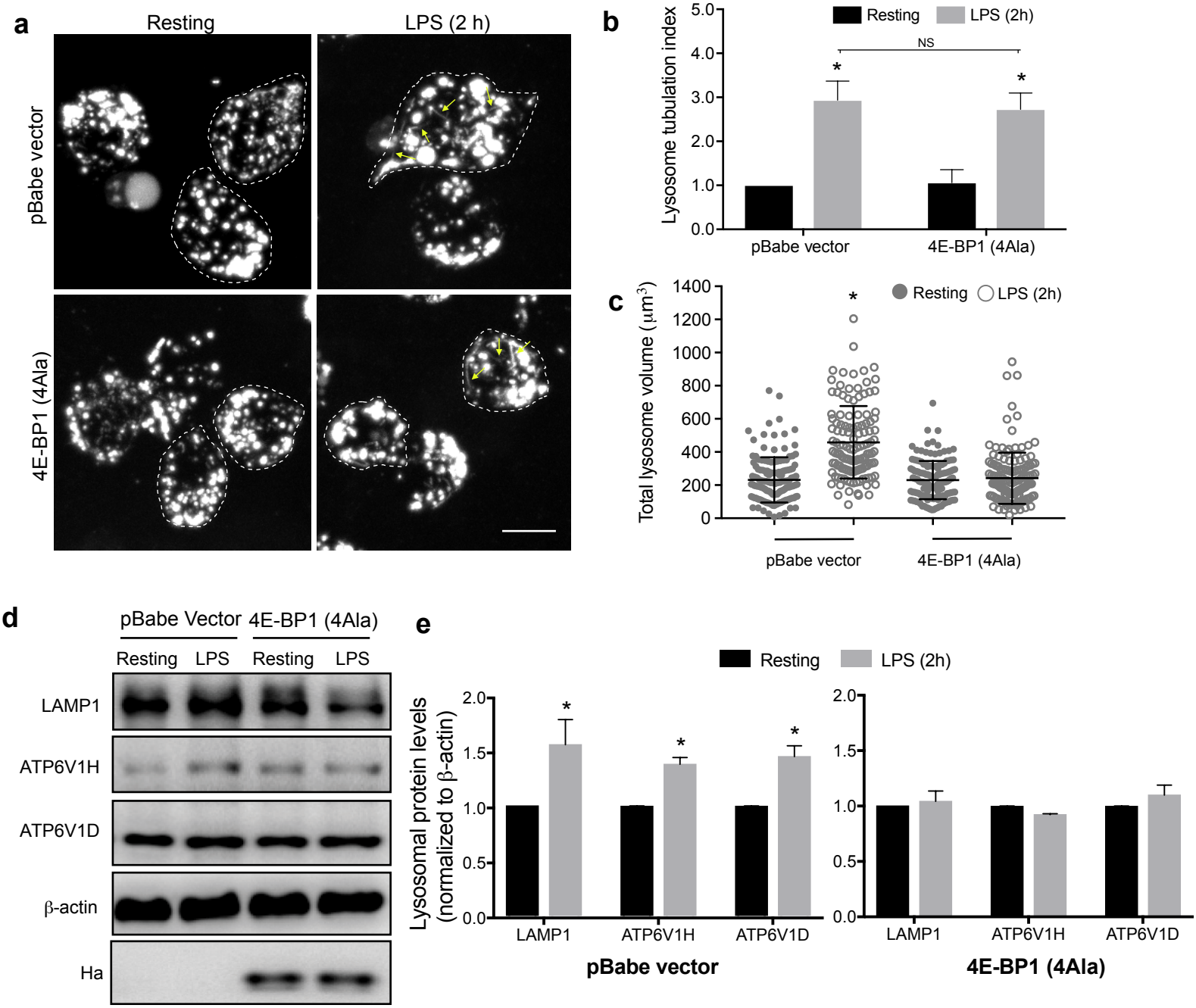

Figure 10